

1 **ACTIVE FLUX METHODS FOR HYPERBOLIC CONSERVATION**
2 **LAWS – FLUX VECTOR SPLITTING AND**
3 **BOUND-PRESERVATION: ONE-DIMENSIONAL CASE ***

4 JUNMING DUAN[†], WASILIJ BARSUKOW[‡], AND CHRISTIAN KLINGENBERG[§]

5 **Abstract.** The active flux (AF) method is a compact high-order finite volume method that
6 evolves cell averages and point values at cell interfaces independently. Within the method of lines
7 framework, the point value can be updated based on Jacobian splitting (JS), incorporating the up-
8 wind idea. However, such JS-based AF methods encounter transonic issues for nonlinear problems
9 due to inaccurate upwind direction estimation. This paper proposes to use flux vector splitting for
10 the point value update, offering a natural and uniform remedy to the transonic issue. To improve
11 robustness, this paper also develops bound-preserving (BP) AF methods for one-dimensional hyper-
12 bolic conservation laws. Two cases are considered: preservation of the maximum principle for the
13 scalar case, and preservation of positive density and pressure for the compressible Euler equations.
14 The update of the cell average in high-order AF methods is rewritten as a convex combination of us-
15 ing the original high-order fluxes and robust low-order (local Lax-Friedrichs or Rusanov) fluxes, and
16 the desired bounds are enforced by choosing the right amount of low-order fluxes. A similar blending
17 strategy is used for the point value update. Several challenging benchmark tests are conducted to
18 verify the accuracy, BP properties, and shock-capturing ability of the methods.

19 **Key words.** Hyperbolic conservation laws, finite volume method, active flux, flux vector split-
20 ting, bound-preserving, convex limiting, scaling limiter

21 **MSC codes.** 65M08, 65M12, 65M20, 35L65

22 **1. Introduction.** This paper is concerned with solving systems of hyperbolic
23 conservation laws

24 (1.1)
$$\frac{\partial \mathbf{U}(x,t)}{\partial t} + \frac{\partial \mathbf{F}(\mathbf{U})}{\partial x} = 0, \quad \mathbf{U}(x,0) = \mathbf{U}_0(x), \quad (x,t) \in \mathbb{R} \times \mathbb{R}^+,$$

25 where $\mathbf{U} \in \mathbb{R}^m$ is the vector of m conservative variables, $\mathbf{F} \in \mathbb{R}^m$ is the physical flux,
26 and $\mathbf{U}_0(x)$ is assumed to be initial data of bounded variation. In this paper, we would
27 like to consider two cases. The first is a scalar conservation law ($m = 1$)

28 (1.2)
$$\frac{\partial u}{\partial t} + \frac{\partial f(u)}{\partial x} = 0, \quad u(x,0) = u_0(x).$$

29 The second case is that of compressible Euler equations of gas dynamics with $\mathbf{U} =$
30 $(\rho, \rho v, E)^\top$ and $\mathbf{F} = (\rho v, \rho v^2 + p, (E + p)v)^\top$, i.e.,

31 (1.3)
$$\frac{\partial}{\partial t} \begin{pmatrix} \rho \\ \rho v \\ E \end{pmatrix} + \frac{\partial}{\partial x} \begin{pmatrix} \rho v \\ \rho v^2 + p \\ (E + p)v \end{pmatrix} = \mathbf{0}, \quad (\rho, v, p)(x,0) = (\rho_0, v_0, p_0).$$

*Submitted to the editors DATE.

Funding: JD was supported by an Alexander von Humboldt Foundation Research fellowship CHN-1234352-HFST-P. CK and WB acknowledge funding by the Deutsche Forschungsgemeinschaft (DFG, German Research Foundation) within *SPP 2410 Hyperbolic Balance Laws in Fluid Mechanics: Complexity, Scales, Randomness (CoScaRa)*, project number 525941602.

[†]Corresponding author. Institute of Mathematics, University of Würzburg, Emil-Fischer-Straße 40, 97074 Würzburg, Germany (junming.duan@uni-wuerzburg.de).

[‡]Institut de Mathématiques de Bordeaux (IMB), CNRS UMR 5251, University of Bordeaux, 33405 Talence, France (wasilij.barsukow@math.u-bordeaux.fr).

[§]Institute of Mathematics, University of Würzburg, Emil-Fischer-Straße 40, 97074 Würzburg, Germany (christian.klingenberg@uni-wuerzburg.de).

32 Here ρ denotes the density, v the velocity, p the pressure, and $E = \frac{1}{2}\rho v^2 + \rho e$ the
 33 total energy with e the specific internal energy. The system (1.3) should be closed by
 34 an equation of state (EOS). This paper considers the perfect gas EOS, $p = (\gamma - 1)\rho e$,
 35 with the adiabatic index $\gamma > 1$. Note that this paper uses bold symbols to refer to
 36 vectors and matrices, such that they are easier to distinguish from scalars.

37 The active flux (AF) method is a new finite volume method [14, 13, 15, 35], that
 38 Roe took inspiration by [40]. Apart from cell averages, it incorporates additional de-
 39 grees of freedom as point values located at the cell interfaces, evolved independently
 40 from the cell average. The original AF method gives a global continuous represen-
 41 tation of the numerical solution using a piecewise quadratic reconstruction, leading
 42 naturally to a third-order accurate method with a compact stencil. The introduc-
 43 tion of point values at the cell interfaces avoids the usage of Riemann solvers as in
 44 usual Godunov methods, because the numerical solution is continuous across the cell
 45 interface and the numerical flux for the cell average update is available directly.

46 The independence of the point value update adds flexibility to the AF methods.
 47 Based on the evolution of the point value, there are generally two kinds of AF methods.
 48 The original one uses exact or approximate evolution operators and Simpson's rule for
 49 flux quadrature in time, i.e. it does not require time integration methods like Runge-
 50 Kutta methods. Exact evolution operators have been studied for linear equations
 51 in [8, 16, 15, 40]. Approximate evolution operators have been explored for Burgers'
 52 equation [14, 13, 35, 5], the compressible Euler equations in one spatial dimension
 53 [14, 26, 5], and hyperbolic balance laws [7, 6], etc. One of the advantages of the AF
 54 method over standard finite volume methods is its structure-preserving property. For
 55 instance, it preserves the vorticity and stationary states for multi-dimensional acoustic
 56 equations [8], and it is naturally well-balanced for acoustics with gravity [7].

57 Since it may not be convenient to derive exact or approximate evolution operators
 58 for nonlinear systems, especially in multi-dimensions, another kind of generalized
 59 AF method was presented in [1, 2, 4]. A method of lines was used, where the cell
 60 average and point value updates are written in semi-discrete form and advanced in
 61 time with time integration methods. In the point values update, the Jacobian matrix
 62 is split based on the sign of the eigenvalues (Jacobian splitting (JS)), and upwind-
 63 biased stencils are used to compute the approximation of derivatives. There are some
 64 deficiencies of the JS when used for the AF methods, e.g., the transonic issue [26] for
 65 nonlinear problems, leading to spikes in the cell average. Some remedies are suggested
 66 in the literature, e.g., using discontinuous reconstruction [26] or evaluating the upwind
 67 direction using more information from the neighbors [5].

68 Solutions to hyperbolic systems (1.1) often stay in an *admissible state set* \mathcal{G} , also
 69 called the invariant domain. For instance, the solutions to initial value problems of
 70 scalar conservation laws (1.2) satisfy a strict maximum principle (MP) [12], i.e.,

$$71 \quad (1.4) \quad \mathcal{G} = \{u \mid m_0 \leq u \leq M_0\}, \quad m_0 = \min_x u_0(x), \quad M_0 = \max_x u_0(x).$$

72 Physically, both the density and pressure in the solutions to the compressible Euler
 73 equations (1.3) should stay positive, i.e.,

$$74 \quad (1.5) \quad \mathcal{G} = \left\{ \mathbf{U} = (\rho, \rho v, E) \mid \rho > 0, \quad p = (\gamma - 1) \left(E - \frac{(\rho v)^2}{2\rho} \right) > 0 \right\}.$$

75 Throughout this paper, it is assumed that \mathcal{G} is a *convex* set, which is obvious for the
 76 scalar case (1.4) and can be verified for the Euler equations (1.5), see e.g. [47]. It is
 77 desirable to conceive so-called bound-preserving (BP) methods, i.e., those guaranteeing

78 that the numerical solutions at a later time will stay in \mathcal{G} , if the initial numerical solu-
 79 tions belong to \mathcal{G} . The BP property of numerical methods is very important for both
 80 theoretical analysis and numerical stability. Many BP methods have been developed
 81 in the past few decades, e.g., a series of works by Shu and collaborators [46, 27, 44],
 82 a recent general framework on BP methods [43], and the convex limiting approach
 83 [18, 23, 30], which can be traced back to the flux-corrected transport (FCT) schemes
 84 for scalar conservation laws [11, 21, 33, 31]. The previous studies on the AF methods
 85 pay limited attention to high-speed flows, or problems containing strong discontinu-
 86 ities, with some efforts on the limiting for the point value update, see e.g. [5, 9].
 87 However, those limitings are not enough to guarantee the BP property, as shown in
 88 our numerical tests. In a very recent paper, the MOOD [10] based stabilization was
 89 adopted to achieve the BP property [3] in an a posteriori fashion.

90 This paper presents a new way for the point value update to cure the transonic
 91 issue and develops suitable BP limiting strategies for the AF methods. The main
 92 contributions and findings in this work can be summarized as follows.

93 i). We propose to employ the flux vector splitting (FVS) methods for the point value
 94 update to cure the transonic issue, since it borrows information from the neighbors
 95 naturally and uniformly. The FVS was originally used to identify the upwind direc-
 96 tions, which is simpler and somewhat more efficient than Godunov-type methods for
 97 solving hyperbolic systems [39]. In our numerical tests, the FVS is also shown to
 98 give better results than the JS, especially the local Lax-Friedrichs (LLF) or Rusanov
 99 FVS, in terms of the CFL number and shock-capturing ability. The FVS can also
 100 cure some defects in two dimensions observed in the JS, which will be shown in our
 101 future companion paper.

102 ii). We design BP limitings for both the update of the cell average and the point value
 103 by blending the high-order AF methods with the first-order LLF method in a convex
 104 combination. The convex limiting [18, 23, 30] and the scaling limiter [32] are applied
 105 to the cell average and point value updates, respectively. The main idea is to retain as
 106 much as possible of the high-order method while guaranteeing the numerical solutions
 107 to be BP, and the blending coefficients are computed by enforcing the bounds. We
 108 show that using a suitable time step size and BP limitings, the numerical solutions
 109 of the BP AF methods satisfy the MP for scalar conservation laws, and give positive
 110 density and pressure for the compressible Euler equations.

111 iii). Several challenging test cases such as the LeBlanc and double rarefaction Rie-
 112 mann problems, the Sedov point blast wave, and blast wave interaction problems are
 113 conducted to demonstrate the BP properties and the shock-capturing ability, which
 114 are rare in the literature for the AF methods.

115 The remainder of this paper is structured as follows. Section 2 introduces the
 116 AF methods based on the JS or FVS for the point value update, and the power
 117 law reconstruction for limiting the derivatives in the point value update. To design
 118 BP methods, Section 3 describes our convex limiting approach for the cell average,
 119 while Section 4 deals with the limiting for the point value. Some numerical tests are
 120 conducted in Section 5 to experimentally demonstrate the accuracy, BP properties,
 121 and shock-capturing ability of the methods. Section 6 concludes the paper with final
 122 remarks and future directions.

123 **2. 1D active flux methods for hyperbolic conservation laws.** This section
 124 presents the 1D semi-discrete AF methods for the hyperbolic conservation laws (1.1),
 125 based on the JS [2] or FVS for the point value update. The fully-discrete methods
 126 are obtained using Runge-Kutta methods.

127 Assume that a 1D computational domain is divided into N cells $I_i = [x_{i-\frac{1}{2}}, x_{i+\frac{1}{2}}]$
 128 with cell centers $x_i = (x_{i-\frac{1}{2}} + x_{i+\frac{1}{2}})/2$ and cell sizes $\Delta x_i = x_{i+\frac{1}{2}} - x_{i-\frac{1}{2}}$, $i = 1, \dots, N$.
 129 The degrees of freedom of the AF methods are the approximations to cell averages
 130 of the conservative variable as well as point values at the cell interfaces, allowing
 131 some freedom in the choice of the point values, e.g. conservative variables, primitive
 132 variables, entropy variables, etc. This paper only considers using the conservative
 133 variables, and the degrees of freedom are denoted by

$$134 \quad (2.1) \quad \bar{U}_i(t) = \frac{1}{\Delta x_i} \int_{I_i} \mathbf{U}(x, t) \, dx, \quad \mathbf{U}_{i+\frac{1}{2}}(t) = \mathbf{U}(x_{i+\frac{1}{2}}, t).$$

135 The cell average is updated by integrating (1.1) over I_i in the following semi-discrete
 136 finite volume manner

$$137 \quad (2.2) \quad \frac{d\bar{U}_i}{dt} = -\frac{1}{\Delta x_i} \left[\mathbf{F}(\mathbf{U}_{i+\frac{1}{2}}) - \mathbf{F}(\mathbf{U}_{i-\frac{1}{2}}) \right].$$

138 Thus, the accuracy of (2.2) is determined by the approximation accuracy of the point
 139 values. It was so far (e.g. in [2]) considered sufficient to update the point values with
 140 any finite-difference-like formula

$$141 \quad (2.3) \quad \frac{d\mathbf{U}_{i+\frac{1}{2}}}{dt} = -\mathcal{R} \left(\mathbf{U}_{i+\frac{1}{2}-l_1}(t), \bar{U}_{i+1-l_1}(t), \dots, \bar{U}_{i+l_2}(t), \mathbf{U}_{i+\frac{1}{2}+l_2}(t) \right), \quad l_1, l_2 \geq 0,$$

142 with \mathcal{R} a consistent approximation of $\partial \mathbf{F} / \partial x$ at $x_{i+\frac{1}{2}}$, as long as it gave rise to a
 143 stable method. This paper explores further conditions on \mathcal{R} for nonlinear problems.

144 **2.1. Point value update using Jacobian splitting.** For smooth solutions,
 145 we have an equivalent formulation in the form

$$146 \quad (2.4) \quad \frac{\partial \mathbf{U}}{\partial t} + \mathbf{J}(\mathbf{U}) \frac{\partial \mathbf{U}}{\partial x} = 0, \quad \mathbf{J}(\mathbf{U}) = \frac{\partial \mathbf{F}(\mathbf{U})}{\partial \mathbf{U}}.$$

147 Inspired by the upwind scheme, (2.4) can be discretized by the JS [1, 2] as follows

$$148 \quad (2.5) \quad \frac{d\mathbf{U}_{i+\frac{1}{2}}}{dt} = - \left[\mathbf{J}^+(\mathbf{U}_{i+\frac{1}{2}}) \mathbf{D}_{i+\frac{1}{2}}^+(\mathbf{U}) + \mathbf{J}^-(\mathbf{U}_{i+\frac{1}{2}}) \mathbf{D}_{i+\frac{1}{2}}^-(\mathbf{U}) \right],$$

149 where the splitting of the Jacobian matrix $\mathbf{J} = \mathbf{J}^+ + \mathbf{J}^-$ is defined as

$$150 \quad \mathbf{J}^+ = \mathbf{R} \mathbf{\Lambda}^+ \mathbf{R}^{-1}, \quad \mathbf{J}^- = \mathbf{R} \mathbf{\Lambda}^- \mathbf{R}^{-1},$$

$$151 \quad \mathbf{\Lambda}^+ = \text{diag}\{\max(\lambda_1, 0), \dots, \max(\lambda_m, 0)\},$$

$$152 \quad \mathbf{\Lambda}^- = \text{diag}\{\min(\lambda_1, 0), \dots, \min(\lambda_m, 0)\},$$

154 based on the eigendecomposition $\partial \mathbf{F} / \partial \mathbf{U} = \mathbf{R} \mathbf{\Lambda} \mathbf{R}^{-1}$, $\mathbf{\Lambda} = \text{diag}\{\lambda_1, \dots, \lambda_m\}$, where
 155 $\lambda_1, \dots, \lambda_m$ are the eigenvalues, with the columns of \mathbf{R} the corresponding eigenvectors.

156 To derive the approximation of the derivatives in (2.5), one can first obtain a high-
 157 order reconstruction for \mathbf{U} in the upwind cell, and then differentiate the reconstructed
 158 polynomial. As an example, a parabolic reconstruction in cell i is

$$159 \quad \mathbf{U}_{\text{para},1}(x) = -3(2\bar{U}_i - \mathbf{U}_{i-\frac{1}{2}} - \mathbf{U}_{i+\frac{1}{2}}) \frac{x^2}{\Delta x_i^2} + (\mathbf{U}_{i+\frac{1}{2}} - \mathbf{U}_{i-\frac{1}{2}}) \frac{x}{\Delta x_i}$$

$$160 \quad (2.6) \quad + \frac{1}{4}(6\bar{U}_i - \mathbf{U}_{i-\frac{1}{2}} - \mathbf{U}_{i+\frac{1}{2}})$$

162 satisfying $\mathbf{U}_{\text{para},1}(\pm\Delta x_i/2) = \mathbf{U}_{i\pm\frac{1}{2}}$, $\frac{1}{\Delta x_i} \int_{-\Delta x_i/2}^{\Delta x_i/2} \mathbf{U}_{\text{para},1}(x) dx = \bar{\mathbf{U}}_i$. Then the de-
 163 rivatives are

$$164 \quad (2.7a) \quad \mathbf{D}_{i+\frac{1}{2}}^+(\mathbf{U}) = \mathbf{U}'_{\text{para},1}(\Delta x_i/2) = \frac{1}{\Delta x_i} \left(2\mathbf{U}_{i-\frac{1}{2}} - 6\bar{\mathbf{U}}_i + 4\mathbf{U}_{i+\frac{1}{2}} \right),$$

$$165 \quad (2.7b) \quad \mathbf{D}_{i+\frac{1}{2}}^-(\mathbf{U}) = \frac{1}{\Delta x_{i+1}} \left(-4\mathbf{U}_{i+\frac{1}{2}} + 6\bar{\mathbf{U}}_{i+1} - 2\mathbf{U}_{i+\frac{3}{2}} \right).$$

167 They are third-order accurate. Higher-order extensions can be obtained by higher-
 168 order finite difference formulae using a larger spatial stencil, see [2] for examples.

169 **2.2. Point value update using flux vector splitting.** One of the deficiencies
 170 of using the JS is the transonic issue that appears for nonlinear problems, as observed
 171 in [26, 5] and described in more detail next. Consider [Example 5.2](#), where we solve
 172 Burgers' equation with a square wave as the initial data. [Figure 3](#) shows the cell
 173 averages and point values based on the JS with 200 cells, as well as the reference
 174 solution. The numerical solution based on the JS without limiting gives a spike at
 175 the initial discontinuity $x = 0.2$, which grows linearly in time. The reason for this
 176 behaviour is the inaccurate estimation of the upwind direction at the cell interface.
 177 In this example, there are two successive point values with different initial data near
 178 the initial discontinuity, denoted by $u_{i-\frac{1}{2}} = 2$, $u_{i+\frac{1}{2}} = -1$, respectively. At the cell
 179 interface $x_{i-\frac{1}{2}}$ or $x_{i+\frac{1}{2}}$, the upwind discretization in (2.7) only uses the data from the
 180 left or right, leading to zero derivatives, thus the point values $u_{i-\frac{1}{2}}$ and $u_{i+\frac{1}{2}}$ stay
 181 unchanged. However, according to the update of the cell average (2.2), \bar{u}_i increases
 182 gradually (which is the observed spike). This deficiency cannot be eliminated by
 183 limitings, as one observes from [Figure 3](#). Some remedies have been proposed, such
 184 as using discontinuous reconstruction [26] and an ‘‘entropy fix’’ that evaluates the
 185 upwind direction not only at the corresponding cell interface but also with values
 186 from its neighbors [5].

187 In this paper, we propose to use the FVS for the point value update, which
 188 borrows the information from the neighbors naturally, still based on the continuous
 189 reconstruction, and can eliminate the generation of the spike effectively, as shown in
 190 [Figure 4](#). The FVS for the point value update reads

$$191 \quad (2.8) \quad \frac{d\mathbf{U}_{i+\frac{1}{2}}}{dt} = - \left[\tilde{\mathbf{D}}^+ \mathbf{F}^+(\mathbf{U}) + \tilde{\mathbf{D}}^- \mathbf{F}^-(\mathbf{U}) \right]_{i+\frac{1}{2}},$$

192 where the flux \mathbf{F} is split into the positive and negative parts $\mathbf{F} = \mathbf{F}^+ + \mathbf{F}^-$ satisfying

$$193 \quad (2.9) \quad \lambda \left(\frac{\partial \mathbf{F}^+}{\partial \mathbf{U}} \right) \geq 0, \quad \lambda \left(\frac{\partial \mathbf{F}^-}{\partial \mathbf{U}} \right) \leq 0,$$

194 i.e., all the eigenvalues of $\frac{\partial \mathbf{F}^+}{\partial \mathbf{U}}$ and $\frac{\partial \mathbf{F}^-}{\partial \mathbf{U}}$ are non-negative and non-positive, respec-
 195 tively. Different FVS can be adopted as long as they satisfy the constraint (2.9),
 196 to be discussed later. Finite difference formulae to approximate the flux derivatives
 197 are obtained similarly to the computation of the derivatives in the JS. A parabolic
 198 reconstruction of the flux can be obtained based on the three flux values as follows

$$199 \quad \mathbf{F}_{\text{para},2}(x) = 2(\mathbf{F}_{i-\frac{1}{2}} - 2\mathbf{F}_i + \mathbf{F}_{i+\frac{1}{2}}) \frac{x^2}{\Delta x_i^2} + (\mathbf{F}_{i+\frac{1}{2}} - \mathbf{F}_{i-\frac{1}{2}}) \frac{x}{\Delta x_i} + \mathbf{F}_i,$$

200 satisfying $\mathbf{F}_{\text{para},2}(\pm\Delta x_i/2) = \mathbf{F}_{i\pm\frac{1}{2}}$, $\mathbf{F}_{\text{para},2}(0) = \mathbf{F}_i$, with $\mathbf{F}_{i\pm\frac{1}{2}} = \mathbf{F}(\mathbf{U}_{i\pm\frac{1}{2}})$, and the
 201 cell-centered point value $\mathbf{F}_i = \mathbf{F}(\mathbf{U}_i)$ is obtained by evaluating the reconstruction

202 of \mathbf{U} , i.e. according to Simpson's rule $\mathbf{U}_i = (-\mathbf{U}_{i-\frac{1}{2}} + 6\bar{\mathbf{U}}_i - \mathbf{U}_{i+\frac{1}{2}})/4$. Then the
203 derivatives are

$$204 \quad (2.10a) \quad \left(\tilde{\mathbf{D}}^+ \mathbf{F}^+\right)_{i+\frac{1}{2}} = \mathbf{F}'_{\text{para},2}(\Delta x_i/2) = \frac{1}{\Delta x_i} \left(\mathbf{F}_{i-\frac{1}{2}} - 4\mathbf{F}_i + 3\mathbf{F}_{i+\frac{1}{2}}\right),$$

$$205 \quad (2.10b) \quad \left(\tilde{\mathbf{D}}^- \mathbf{F}^-\right)_{i+\frac{1}{2}} = \frac{1}{\Delta x_{i+1}} \left(-3\mathbf{F}_{i+\frac{1}{2}} + 4\mathbf{F}_{i+1} - \mathbf{F}_{i+\frac{3}{2}}\right).$$

207 These finite differences are third-order accurate. While the reconstructions of both \mathbf{U}
208 and \mathbf{F} are parabolic, the coefficients in the formula (2.10) differ from (2.7) because
209 (2.10) uses the cell-centered value rather than the cell average. Our numerical tests in
210 Section 5 show that the AF methods based on the FVS generally give better results
211 than the JS.

212 **2.2.1. Local Lax-Friedrichs flux vector splitting.** The first FVS we consider
213 is the LLF FVS, defined as

$$214 \quad \mathbf{F}^\pm = \frac{1}{2}(\mathbf{F}(\mathbf{U}) \pm \alpha \mathbf{U}),$$

215 where the choice of α should fulfill (2.9) across the spatial stencil. In our implemen-
216 tation, it is determined by

$$217 \quad (2.11) \quad \alpha_{i+\frac{1}{2}} = \max_{r,\ell} \{|\lambda_\ell(\mathbf{U}_r)|\}, \quad r \in \left\{i - \frac{1}{2}, i, i + \frac{1}{2}, i + 1, u + \frac{3}{2}\right\}, \quad \ell = 1, \dots, m.$$

218 One can also choose α to be the maximal absolute value of the eigenvalues in the whole
219 domain, corresponding to the (global) LF splitting. Note, however, that a larger α
220 generally leads to a smaller time step size and more dissipation.

221 **2.2.2. Upwind flux vector splitting.** One can also split the Jacobian matrix
222 based on each characteristic field,

$$223 \quad (2.12) \quad \mathbf{F}^\pm = \frac{1}{2}(\mathbf{F}(\mathbf{U}) \pm |\mathbf{J}|\mathbf{U}), \quad |\mathbf{J}| = \mathbf{R}(\mathbf{\Lambda}^+ - \mathbf{\Lambda}^-)\mathbf{R}^{-1}.$$

224 For linear systems, one has $\mathbf{F} = \mathbf{J}\mathbf{U}$, so (2.12) reduces to the JS. To be specific,

$$225 \quad \mathbf{F}^\pm = \frac{1}{2}(\mathbf{J} \pm |\mathbf{J}|)\mathbf{U} = \mathbf{R}\mathbf{\Lambda}^\pm \mathbf{R}^{-1}\mathbf{U} = \mathbf{J}^\pm \mathbf{U},$$

226 with \mathbf{J}^\pm a constant matrix so that $\tilde{\mathbf{D}}^\pm \mathbf{F}^\pm(\mathbf{U}) = \mathbf{J}^\pm \tilde{\mathbf{D}}^\pm \mathbf{U}$, which is the same as
227 $\mathbf{J}^\pm \mathbf{D}^\pm \mathbf{U}$ if \mathbf{D}^+ and $\tilde{\mathbf{D}}^+$ are derived from the same reconstructed polynomial. In
228 other words, the AF methods using this FVS enjoy the same properties as the original
229 JS-based AF methods for linear systems.

230 Such an FVS is also known as the Steger-Warming (SW) FVS [37] for the Euler
231 equations (1.3), since the ‘‘homogeneity property’’ holds [39], i.e., $\mathbf{F} = \mathbf{J}\mathbf{U}$. One can
232 write down the SW FVS explicitly

$$233 \quad \mathbf{F}^\pm = \begin{bmatrix} \frac{\rho}{2\gamma} \alpha^\pm \\ \frac{\rho}{2\gamma} (\alpha^\pm v + a(\lambda_2^\pm - \lambda_3^\pm)) \\ \frac{\rho}{2\gamma} \left(\frac{1}{2}\alpha^\pm v^2 + av(\lambda_2^\pm - \lambda_3^\pm) + \frac{a^2}{\gamma-1}(\lambda_2^\pm + \lambda_3^\pm)\right) \end{bmatrix},$$

235 where $\lambda_1 = v$, $\lambda_2 = v + a$, $\lambda_3 = v - a$, $\alpha^\pm = 2(\gamma - 1)\lambda_1^\pm + \lambda_2^\pm + \lambda_3^\pm$, and $a = \sqrt{\gamma p/\rho}$
236 is the sound speed.

237 **2.2.3. Van Leer-Hänel flux vector splitting for the Euler equations.**

238 Another popular FVS for the Euler equations was proposed by Van Leer [41], and
 239 improved by [24]. The flux can be split based on the Mach number $M = v/a$ as

$$240 \quad \mathbf{F} = \begin{bmatrix} \rho a M \\ \rho a^2 (M^2 + \frac{1}{\gamma}) \\ \rho a^3 M (\frac{1}{2} M^2 + \frac{1}{\gamma-1}) \end{bmatrix} = \mathbf{F}^+ + \mathbf{F}^-, \quad \mathbf{F}^\pm = \begin{bmatrix} \pm \frac{1}{4} \rho a (M \pm 1)^2 \\ \pm \frac{1}{4} \rho a (M \pm 1)^2 v + p^\pm \\ \pm \frac{1}{4} \rho a (M \pm 1)^2 H \end{bmatrix},$$

241 with the enthalpy $H = (E + p)/\rho$, and the pressure splitting $p^\pm = \frac{1}{2}(1 \pm \gamma M)p$. This
 242 FVS gives a quadratic differentiable splitting with respect to the Mach number.

243 **2.3. 1D power law reconstruction for point value update.** When the
 244 numerical solutions contain discontinuities, the computation of the derivatives (2.7)
 245 or (2.10) based on the parabolic reconstructions may cause oscillations. Thus, it is
 246 reasonable to seek finite difference approximations based on differentiating a modified
 247 reconstruction with improved monotonicity properties. This section only considers
 248 the scalar case and can be extended to systems of equations in a component-wise
 249 fashion.

250 The power law reconstruction proposed in [5] can be used to replace the original
 251 parabolic reconstruction to achieve monotonicity on some occasions. It is shown in
 252 Theorem 5 in [5] that the extremum is not avoidable in the cell $I_i = [x_{i-\frac{1}{2}}, x_{i+\frac{1}{2}}]$
 253 for continuous reconstructions if the cell average lies outside the range of the point
 254 values $(\bar{u}_i - u_{i-\frac{1}{2}})(u_{i+\frac{1}{2}} - \bar{u}_i) < 0$. The parabola is monotone, and thus no action
 255 is required when $(2u_{i-\frac{1}{2}} + u_{i+\frac{1}{2}})/3 < \bar{u}_i < (u_{i-\frac{1}{2}} + 2u_{i+\frac{1}{2}})/3$ or $(2u_{i-\frac{1}{2}} + u_{i+\frac{1}{2}})/3 >$
 256 $\bar{u}_i > (u_{i-\frac{1}{2}} + 2u_{i+\frac{1}{2}})/3$. Upon defining $r = \frac{u_{i+1/2} - \bar{u}_i}{\bar{u}_i - u_{i-1/2}}$, one can equivalently express
 257 that the parabola is monotone when $1/2 < r < 2$. In both these cases, the parabolic
 258 reconstruction is used, and the derivatives are obtained by (2.7) or (2.10). Otherwise,
 259 the following power law reconstruction is used.

260 PROPOSITION 2.1 (Barsukow [5]). The power law reconstruction

$$261 \quad (2.13) \quad \begin{cases} u_{\text{pw1},1}(x) = u_{i-\frac{1}{2}} + (u_{i+\frac{1}{2}} - u_{i-\frac{1}{2}}) \left(\frac{x - x_i}{\Delta x_i} + \frac{1}{2} \right)^r, & \text{if } r > 2 \\ u_{\text{pw1},2}(x) = u_{i+\frac{1}{2}} - (u_{i+\frac{1}{2}} - u_{i-\frac{1}{2}}) \left(\frac{1}{2} - \frac{x - x_i}{\Delta x_i} \right)^{1/r}, & \text{if } 0 < r < 1/2 \end{cases}$$

262 is monotone and satisfies

$$263 \quad u_{\text{pw1},l}(x_{i-\frac{1}{2}}) = u_{i-\frac{1}{2}}, \quad u_{\text{pw1},l}(x_{i+\frac{1}{2}}) = u_{i+\frac{1}{2}}, \quad \frac{1}{\Delta x_i} \int_{I_i} u_{\text{pw1},l}(x) \, dx = \bar{u}_i, \quad l = 1, 2.$$

264 A comparison between the parabolic reconstruction (2.6) and power law recon-
 265 struction (2.13) is given in Figure 1 with point values fixed as -1 and 1 at the inter-
 266 faces, and different cell averages $\{-1.1, -0.8, -1/3, 0.1, 1/3, 0.8, 1.1\}$. One can observe
 267 monotone profiles for the power law reconstruction when the cell average lies between
 268 the two point values. Based on (2.13), the derivatives can be computed directly

$$269 \quad \begin{cases} u'_{\text{pw1},1}(x) = \frac{u_{i+\frac{1}{2}} - u_{i-\frac{1}{2}}}{\Delta x_i} r \left(\frac{x - x_i}{\Delta x_i} + \frac{1}{2} \right)^{r-1}, & \text{if } r > 2, \\ u'_{\text{pw1},2}(x) = \frac{u_{i+\frac{1}{2}} - u_{i-\frac{1}{2}}}{\Delta x_i} \frac{1}{r} \left(\frac{1}{2} - \frac{x - x_i}{\Delta x_i} \right)^{1/r-1}, & \text{if } 0 < r < 1/2. \end{cases}$$

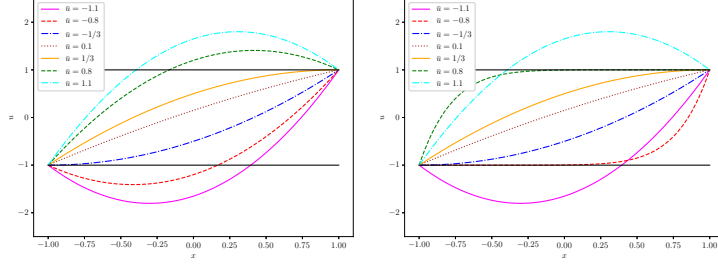


Fig. 1: The parabolic (2.6) and power law reconstruction (2.13) obtained with different cell averages $\{-1.1, -0.8, -1/3, 0.1, 1/3, 0.8, 1.1\}$, and fixed point values as -1 and 1 at the left and right interfaces.

270 At the left interface, the derivative is

$$271 \quad (2.14) \quad \begin{cases} u'_{pw1,1}(x_{i-\frac{1}{2}}^+) = 0, & \text{if } r > 2, \\ u'_{pw1,2}(x_{i-\frac{1}{2}}^+) = \frac{u_{i+\frac{1}{2}} - u_{i-\frac{1}{2}}}{\Delta x_i} \frac{1}{r}, & \text{if } 0 < r < 1/2, \end{cases}$$

272 and at the right interface, the derivative is

$$273 \quad (2.15) \quad \begin{cases} u'_{pw1,1}(x_{i+\frac{1}{2}}^-) = \frac{u_{i+\frac{1}{2}} - u_{i-\frac{1}{2}}}{\Delta x_i} r, & \text{if } r > 2, \\ u'_{pw1,2}(x_{i+\frac{1}{2}}^-) = 0, & \text{if } 0 < r < 1/2. \end{cases}$$

274 To avoid computational issues, when $r \notin [1/50, 50]$, the parabolic reconstruction is
275 adopted directly.

276 For the FVS, as the cell average of the flux can be obtained through Simpson's
277 rule, $\bar{f}_i = (f_{i-\frac{1}{2}} + 4f_i + f_{i+\frac{1}{2}})/6$, the flux derivatives can be computed by (2.14)-(2.15).

278 *Remark 2.2.* In [2], it is mentioned that if the signs of the derivatives of the
279 parabolic reconstruction and the first-order reconstruction are the same, then the
280 parabolic reconstruction is adopted. This strategy is not employed in this paper as
281 the numerical results may be worse.

282 **2.4. Time discretization.** The fully-discrete scheme is obtained by using the
283 SSP-RK3 method [17]

$$284 \quad (2.16) \quad \begin{aligned} \mathbf{U}^* &= \mathbf{U}^n + \Delta t^n \mathbf{L}(\mathbf{U}^n), \\ \mathbf{U}^{**} &= \frac{3}{4} \mathbf{U}^n + \frac{1}{4} (\mathbf{U}^* + \Delta t^n \mathbf{L}(\mathbf{U}^*)), \\ \mathbf{U}^{n+1} &= \frac{1}{3} \mathbf{U}^n + \frac{2}{3} (\mathbf{U}^{**} + \Delta t^n \mathbf{L}(\mathbf{U}^{**})), \end{aligned}$$

285 where \mathbf{L} is the right-hand side of the semi-discrete schemes (2.2) or (2.3). The time
286 step size is determined by the usual CFL condition

$$287 \quad (2.17) \quad \Delta t^n = \frac{C_{\text{CFL}}}{\max_{i,\ell} \{\lambda_\ell(\bar{\mathbf{U}}_i) / \Delta x_i\}}.$$

288 **3. Convex limiting for the cell average.** Although the power law recon-
 289 struction [5] has been shown to effectively reduce spurious oscillations, the numerical
 290 solutions may still violate certain bounds, e.g., the appearance of negative density or
 291 pressure, leading to unphysical solutions or even causing the simulations to blow up.
 292 Since the degrees of freedom in the AF methods include both cell averages and point
 293 values, it is necessary to design suitable BP limitings for both of them to achieve the
 294 BP property. The limiting for the cell average has not been addressed much in the
 295 literature, except for a very recent work [3].

296 **DEFINITION 3.1.** *An AF method is called bound-preserving (BP) if starting from*
 297 *cell averages and point values in the admissible state set \mathcal{G} , the cell averages and point*
 298 *values remain in \mathcal{G} at the next time step.*

299 This section presents a convex limiting approach to achieve the BP property of
 300 the cell average update. The basic idea of the convex limiting approaches [18, 23, 30]
 301 is to enforce the preservation of local and global bounds by constraining individual
 302 numerical fluxes. The BP or invariant domain-preserving (IDP) properties of flux-
 303 limited approximations are shown using representations in terms of intermediate states
 304 that stay in convex admissible state sets [18, 22]. The low-order scheme is chosen as
 305 the first-order LLF scheme

$$306 \quad \bar{U}_i^L = \bar{U}_i^n - \mu_i \left(\hat{F}_{i+\frac{1}{2}}^L - \hat{F}_{i-\frac{1}{2}}^L \right), \quad \mu_i = \Delta t^n / \Delta x_i,$$

$$307 \quad \hat{F}_{i+\frac{1}{2}}^L = \frac{1}{2} \left(F(\bar{U}_i^n) + F(\bar{U}_{i+1}^n) \right) - \frac{\alpha_{i+\frac{1}{2}}}{2} \left(\bar{U}_{i+1}^n - \bar{U}_i^n \right),$$

309 where $\alpha_{i+\frac{1}{2}}$ is an *upper bound* for the maximum wave speed of the Riemann problem
 310 with the initial data U_i, U_{i+1} , whose estimation for scalar conservation laws and the
 311 Euler equations can be found in [20] and [19], respectively. Note that here $\alpha_{i+\frac{1}{2}}$
 312 is not the same as the one in the LLF FVS (2.11). Following [20], the first-order LLF
 313 scheme can be rewritten as

$$314 \quad (3.1) \quad \bar{U}_i^L = \left[1 - \mu_i \left(\alpha_{i-\frac{1}{2}} + \alpha_{i+\frac{1}{2}} \right) \right] \bar{U}_i^n + \mu_i \alpha_{i-\frac{1}{2}} \tilde{U}_{i-\frac{1}{2}} + \mu_i \alpha_{i+\frac{1}{2}} \tilde{U}_{i+\frac{1}{2}},$$

315 with the intermediate states defined as

$$316 \quad (3.2) \quad \tilde{U}_{i-\frac{1}{2}} := \frac{1}{2} \left(\bar{U}_{i-1}^n + \bar{U}_i^n \right) + \frac{1}{2\alpha_{i-\frac{1}{2}}} \left[F(\bar{U}_{i-1}^n) - F(\bar{U}_i^n) \right],$$

$$\tilde{U}_{i+\frac{1}{2}} := \frac{1}{2} \left(\bar{U}_i^n + \bar{U}_{i+1}^n \right) + \frac{1}{2\alpha_{i+\frac{1}{2}}} \left[F(\bar{U}_i^n) - F(\bar{U}_{i+1}^n) \right].$$

317 **Remark 3.2.** As $\alpha_{i+\frac{1}{2}}$ is chosen to be larger than the leftmost and rightmost wave
 318 speed, the intermediate state defined in (3.2) is indeed an average of the exact Riemann
 319 solution [20], thus it belongs to \mathcal{G} . For systems, it is also the intermediate state of the
 320 HLL solver [25]. Moreover, the intermediate state (3.2) preserves all *convex invariants*
 321 (e.g., density and pressure positivity, and minimum entropy principle for the Euler
 322 equations) of initial value problems for hyperbolic systems [20].

323 **LEMMA 3.3** (Guermont and Popov [20]). If the time step size Δt^n satisfies

$$324 \quad (3.3) \quad \Delta t^n \leq \frac{\Delta x_i}{\alpha_{i-\frac{1}{2}} + \alpha_{i+\frac{1}{2}}},$$

325 then (3.1) is a convex combination, and the first-order LLF scheme (3.1) is BP.

326 The proof relies on the fact that the intermediate state (3.2) stays in the admissible
327 state set \mathcal{G} and the convexity of \mathcal{G} .

328 Upon defining the anti-diffusive flux $\Delta\widehat{\mathbf{F}}_{i\pm\frac{1}{2}}^{\text{H}} := \widehat{\mathbf{F}}_{i\pm\frac{1}{2}}^{\text{H}} - \widehat{\mathbf{F}}_{i\pm\frac{1}{2}}^{\text{L}}$ with $\widehat{\mathbf{F}}_{i\pm\frac{1}{2}}^{\text{H}} :=$
329 $\mathbf{F}(\mathbf{U}_{i\pm\frac{1}{2}})$, a forward-Euler step applied to the semi-discrete high-order scheme for
330 the cell average (2.2) can be written as

$$331 \quad \overline{\mathbf{U}}_i^{\text{H}} = \overline{\mathbf{U}}_i^n - \mu_i(\widehat{\mathbf{F}}_{i+\frac{1}{2}}^{\text{H}} - \widehat{\mathbf{F}}_{i-\frac{1}{2}}^{\text{H}}) = \overline{\mathbf{U}}_i^n - \mu_i(\widehat{\mathbf{F}}_{i+\frac{1}{2}}^{\text{L}} - \widehat{\mathbf{F}}_{i-\frac{1}{2}}^{\text{L}}) - \mu_i(\Delta\widehat{\mathbf{F}}_{i+\frac{1}{2}} - \Delta\widehat{\mathbf{F}}_{i-\frac{1}{2}})$$

(3.4)

$$332 \quad =: \left[1 - \mu_i(\alpha_{i-\frac{1}{2}} + \alpha_{i+\frac{1}{2}})\right] \overline{\mathbf{U}}_i^n + \mu_i\alpha_{i-\frac{1}{2}}\widetilde{\mathbf{U}}_{i-\frac{1}{2}}^{\text{H}} + \mu_i\alpha_{i+\frac{1}{2}}\widetilde{\mathbf{U}}_{i+\frac{1}{2}}^{\text{H}},$$

$$333 \quad \widetilde{\mathbf{U}}_{i-\frac{1}{2}}^{\text{H}} := \left(\widetilde{\mathbf{U}}_{i-\frac{1}{2}} + \frac{\Delta\widehat{\mathbf{F}}_{i-\frac{1}{2}}}{\alpha_{i-\frac{1}{2}}}\right), \quad \widetilde{\mathbf{U}}_{i+\frac{1}{2}}^{\text{H}} := \left(\widetilde{\mathbf{U}}_{i+\frac{1}{2}} - \frac{\Delta\widehat{\mathbf{F}}_{i+\frac{1}{2}}}{\alpha_{i+\frac{1}{2}}}\right).$$

334

335 With the low-order scheme (3.1) and high-order scheme (3.4) having the same
336 form one can now define the limited scheme for the cell average as

$$337 \quad (3.5) \quad \overline{\mathbf{U}}_i^{\text{Lim}} = \left[1 - \mu_i(\alpha_{i-\frac{1}{2}} + \alpha_{i+\frac{1}{2}})\right] \overline{\mathbf{U}}_i^n + \mu_i\alpha_{i-\frac{1}{2}}\widetilde{\mathbf{U}}_{i-\frac{1}{2}}^{\text{Lim},+} + \mu_i\alpha_{i+\frac{1}{2}}\widetilde{\mathbf{U}}_{i+\frac{1}{2}}^{\text{Lim},-},$$

338 with the limited intermediate states

$$339 \quad \widetilde{\mathbf{U}}_{i-\frac{1}{2}}^{\text{Lim},+} = \widetilde{\mathbf{U}}_{i-\frac{1}{2}} + \frac{\Delta\widehat{\mathbf{F}}_{i-\frac{1}{2}}^{\text{Lim}}}{\alpha_{i-\frac{1}{2}}} := \widetilde{\mathbf{U}}_{i-\frac{1}{2}} + \frac{\theta_{i-\frac{1}{2}}\Delta\widehat{\mathbf{F}}_{i-\frac{1}{2}}}{\alpha_{i-\frac{1}{2}}},$$

$$340 \quad \widetilde{\mathbf{U}}_{i+\frac{1}{2}}^{\text{Lim},-} = \widetilde{\mathbf{U}}_{i+\frac{1}{2}} - \frac{\Delta\widehat{\mathbf{F}}_{i+\frac{1}{2}}^{\text{Lim}}}{\alpha_{i+\frac{1}{2}}} := \widetilde{\mathbf{U}}_{i+\frac{1}{2}} - \frac{\theta_{i+\frac{1}{2}}\Delta\widehat{\mathbf{F}}_{i+\frac{1}{2}}}{\alpha_{i+\frac{1}{2}}},$$

341

342 where the coefficients $\theta_{i\pm\frac{1}{2}} \in [0, 1]$.

343 PROPOSITION 3.4. If the cell average at the last time step $\overline{\mathbf{U}}_i^n$ and the limited
344 intermediate states $\widetilde{\mathbf{U}}_{i\pm\frac{1}{2}}^{\text{Lim},\mp}$ belong to the admissible state set \mathcal{G} , then the limited
345 average update (3.5) is BP, i.e., $\overline{\mathbf{U}}_i^{\text{Lim}} \in \mathcal{G}$, under the CFL condition (3.3). If the
346 SSP-RK3 (2.16) is used for the time integration, the high-order scheme is also BP.

347 *Proof.* Under the constraint (3.3), the limited cell average update $\overline{\mathbf{U}}_i^{\text{Lim}}$ is a convex
348 combination of $\overline{\mathbf{U}}_i^n$ and $\widetilde{\mathbf{U}}_{i\pm\frac{1}{2}}^{\text{Lim},\mp}$, thus it belongs to \mathcal{G} due to the convexity of \mathcal{G} . Because
349 the SSP-RK3 is a convex combination of forward-Euler stages, the high-order scheme
350 equipped with the SSP-RK3 is also BP according to the convexity. \square

351 *Remark 3.5.* The scheme (3.5) is conservative as it amounts to using the nu-
352 merical flux $\widehat{\mathbf{F}}_{i+\frac{1}{2}}^{\text{L}} + \theta_{i+\frac{1}{2}}\Delta\widehat{\mathbf{F}}_{i+\frac{1}{2}} = \theta_{i+\frac{1}{2}}\widehat{\mathbf{F}}_{i+\frac{1}{2}}^{\text{H}} + (1 - \theta_{i+\frac{1}{2}})\widehat{\mathbf{F}}_{i+\frac{1}{2}}^{\text{L}}$, which is a convex
353 combination of the high-order and low-order fluxes.

354 *Remark 3.6.* It should be noted that the time step size (3.3) is determined based
355 on the solutions at t^n . If the constraint is not satisfied at the later stage of the
356 SSP-RK3, the BP property may not be achieved because (3.5) is no longer a convex
357 combination. In our implementation, we start from the usual CFL condition (2.17).
358 Then, if the high-order AF states need BP limitings and (3.2) is not BP or (3.3) is not
359 satisfied, the numerical solutions are set back to the last time step, and we rerun with
360 a halved time step size until (3.2) is BP and the constraint (3.3) is satisfied. This is
361 also a typical implementation to save computational costs in other BP methods.

362 The remaining task is to determine the coefficients at each interface $\theta_{i\pm\frac{1}{2}}$ such
 363 that $\tilde{U}_{i\pm\frac{1}{2}}^{\text{Lim},\mp} \in \mathcal{G}$ and stay as close as possible to the high-order states $\tilde{U}_{i\pm\frac{1}{2}}^{\text{H}}$, i.e., the
 364 goal is to find the largest $\theta_{i\pm\frac{1}{2}} \in [0, 1]$ such that $\tilde{U}_{i\pm\frac{1}{2}}^{\text{Lim},\mp} \in \mathcal{G}$.

365 **3.1. Application to scalar conservation laws.** This section is devoted to
 366 applying the convex limiting approach to scalar conservation laws (1.2), such that the
 367 numerical solutions satisfy the global or local MP. For the global MP, the blending
 368 coefficient $\theta_{i+\frac{1}{2}} \in [0, 1]$ should be chosen such that $m_0 \leq \tilde{u}_{i+\frac{1}{2}}^{\text{Lim},\pm} \leq M_0$, with m_0, M_0
 369 defined in (1.4), which gives

$$370 \quad \theta_{i+\frac{1}{2}} = \begin{cases} \min \left\{ 1, \frac{\alpha_{i+\frac{1}{2}}(\tilde{u}_{i+\frac{1}{2}} - m_0)}{\Delta \hat{f}_{i+\frac{1}{2}}}, \frac{\alpha_{i+\frac{1}{2}}(M_0 - \tilde{u}_{i+\frac{1}{2}})}{\Delta \hat{f}_{i+\frac{1}{2}}} \right\}, & \text{if } \Delta \hat{f}_{i+\frac{1}{2}} > 0, \\ \min \left\{ 1, \frac{\alpha_{i+\frac{1}{2}}(m_0 - \tilde{u}_{i+\frac{1}{2}})}{\Delta \hat{f}_{i+\frac{1}{2}}}, \frac{\alpha_{i+\frac{1}{2}}(\tilde{u}_{i+\frac{1}{2}} - M_0)}{\Delta \hat{f}_{i+\frac{1}{2}}} \right\}, & \text{if } \Delta \hat{f}_{i+\frac{1}{2}} < 0. \end{cases}$$

371 To avoid a small denominator, the limited anti-diffusive flux can be obtained directly,

$$372 \quad \Delta \hat{f}_{i+\frac{1}{2}}^{\text{Lim}} = \begin{cases} \min \left\{ \Delta \hat{f}_{i+\frac{1}{2}}, \alpha_{i+\frac{1}{2}}(\tilde{u}_{i+\frac{1}{2}} - m_0), \alpha_{i+\frac{1}{2}}(M_0 - \tilde{u}_{i+\frac{1}{2}}) \right\}, & \text{if } \Delta \hat{f}_{i+\frac{1}{2}} \geq 0, \\ \max \left\{ \Delta \hat{f}_{i+\frac{1}{2}}, \alpha_{i+\frac{1}{2}}(m_0 - \tilde{u}_{i+\frac{1}{2}}), \alpha_{i+\frac{1}{2}}(\tilde{u}_{i+\frac{1}{2}} - M_0) \right\}, & \text{otherwise.} \end{cases}$$

373 On the other hand, one can also enforce the local MP $u_i^{\min} \leq \tilde{u}_{i+\frac{1}{2}}^{\text{Lim},-} \leq u_i^{\max}$,
 374 $u_{i+1}^{\min} \leq \tilde{u}_{i+\frac{1}{2}}^{\text{Lim},+} \leq u_{i+1}^{\max}$, which helps to suppress spurious oscillations and improve
 375 shock-capturing ability. The corresponding limited anti-diffusive flux is

$$376 \quad \Delta \hat{f}_{i+\frac{1}{2}}^{\text{Lim}} = \begin{cases} \min \left\{ \Delta \hat{f}_{i+\frac{1}{2}}, \alpha_{i+\frac{1}{2}}(\tilde{u}_{i+\frac{1}{2}} - u_i^{\min}), \alpha_{i+\frac{1}{2}}(u_{i+1}^{\max} - \tilde{u}_{i+\frac{1}{2}}) \right\}, & \text{if } \Delta \hat{f}_{i+\frac{1}{2}} \geq 0, \\ \max \left\{ \Delta \hat{f}_{i+\frac{1}{2}}, \alpha_{i+\frac{1}{2}}(u_{i+1}^{\min} - \tilde{u}_{i+\frac{1}{2}}), \alpha_{i+\frac{1}{2}}(\tilde{u}_{i+\frac{1}{2}} - u_i^{\max}) \right\}, & \text{otherwise.} \end{cases}$$

377 The choice of the local bounds can be based on the intermediate states

$$378 \quad u_i^{\min} = \min \left\{ \tilde{u}_i^n, \tilde{u}_{i-\frac{1}{2}}, \tilde{u}_{i+\frac{1}{2}} \right\}, \quad u_i^{\max} = \max \left\{ \tilde{u}_i^n, \tilde{u}_{i-\frac{1}{2}}, \tilde{u}_{i+\frac{1}{2}} \right\}.$$

379 Finally, the numerical flux is

$$380 \quad (3.6) \quad \hat{f}_{i+\frac{1}{2}}^{\text{Lim}} = \hat{f}_{i+\frac{1}{2}}^{\text{L}} + \Delta \hat{f}_{i+\frac{1}{2}}^{\text{Lim}}.$$

381 **3.2. Application to the compressible Euler equations.** This section aims
 382 at enforcing the strict positivity of density and pressure, i.e., $\rho > \varepsilon$, $p > \varepsilon$, with ε a
 383 small positive number close to zero, chosen as 10^{-13} in our numerical tests.

384 **3.2.1. Positivity of density.** The first step is to impose the density positivity
 385 $\tilde{U}_{i+\frac{1}{2}}^{\text{Lim},\pm,\rho} > \varepsilon$, where $U^{*,\rho}$ denotes the density component of U^* . The corresponding
 386 density component of the limited anti-diffusive flux is

$$387 \quad \Delta \hat{F}_{i+\frac{1}{2}}^{\text{Lim},*,\rho} = \begin{cases} \min \left\{ \Delta \hat{F}_{i+\frac{1}{2}}^{\rho}, \alpha_{i+\frac{1}{2}} \left(\tilde{U}_{i+\frac{1}{2}}^{\rho} - \varepsilon \right) \right\}, & \text{if } \Delta \hat{F}_{i+\frac{1}{2}}^{\rho} \geq 0, \\ \max \left\{ \Delta \hat{F}_{i+\frac{1}{2}}^{\rho}, \alpha_{i+\frac{1}{2}} \left(\varepsilon - \tilde{U}_{i+\frac{1}{2}}^{\rho} \right) \right\}, & \text{otherwise.} \end{cases}$$

388 Then the density component of the limited numerical flux is $\hat{F}_{i+\frac{1}{2}}^{\text{Lim},*,\rho} = \hat{F}_{i+\frac{1}{2}}^{\text{L},\rho} +$
 389 $\Delta \hat{F}_{i+\frac{1}{2}}^{\text{Lim},*,\rho}$, with the other components remaining the same as $\hat{F}_{i+\frac{1}{2}}^{\text{H}}$.

390 **3.2.2. Positivity of pressure.** The second step is to enforce pressure positivity
 391 $p(\tilde{U}_{i+\frac{1}{2}}^{\text{Lim},\pm}) > \varepsilon$, where $p(U^*)$ denotes the pressure recovered from U^* , with

$$392 \quad \tilde{U}_{i+\frac{1}{2}}^{\text{Lim},\pm} = \tilde{U}_{i+\frac{1}{2}} \pm \frac{\theta_{i+\frac{1}{2}} \Delta \hat{F}_{i+\frac{1}{2}}^{\text{Lim},*}}{\alpha_{i+\frac{1}{2}}}, \quad \Delta \hat{F}_{i+\frac{1}{2}}^{\text{Lim},*} = \hat{F}_{i+\frac{1}{2}}^{\text{Lim},*} - \hat{F}_{i+\frac{1}{2}}^{\text{L}}.$$

393 Such constraints lead to two inequalities

$$394 \quad (3.7) \quad \frac{A_{i+\frac{1}{2}}}{\alpha_{i+\frac{1}{2}}^2} \theta_{i+\frac{1}{2}}^2 \pm \frac{B_{i+\frac{1}{2}}}{\alpha_{i+\frac{1}{2}}} \theta_{i+\frac{1}{2}} < C_{i+\frac{1}{2}},$$

395 with the coefficients

$$396 \quad A_{i+\frac{1}{2}} = \frac{1}{2} \left(\Delta \hat{F}_{i+\frac{1}{2}}^{\text{Lim},*,\rho v} \right)^2 - \Delta \hat{F}_{i+\frac{1}{2}}^{\text{Lim},*,\rho} \Delta \hat{F}_{i+\frac{1}{2}}^{\text{Lim},*,E},$$

$$397 \quad B_{i+\frac{1}{2}} = \alpha_{i+\frac{1}{2}} \left(\Delta \hat{F}_{i+\frac{1}{2}}^{\text{Lim},*,\rho} \tilde{U}_{i+\frac{1}{2}}^E + \tilde{U}_{i+\frac{1}{2}}^\rho \Delta \hat{F}_{i+\frac{1}{2}}^{\text{Lim},*,E} - \Delta \hat{F}_{i+\frac{1}{2}}^{\text{Lim},*,\rho v} \tilde{U}_{i+\frac{1}{2}}^{\rho v} - \varepsilon \Delta \hat{F}_{i+\frac{1}{2}}^{\text{Lim},*,\rho} \right),$$

$$398 \quad C_{i+\frac{1}{2}} = \alpha_{i+\frac{1}{2}}^2 \left(\tilde{U}_{i+\frac{1}{2}}^\rho \tilde{U}_{i+\frac{1}{2}}^E - \frac{1}{2} \left(\tilde{U}_{i+\frac{1}{2}}^{\rho v} \right)^2 - \varepsilon \tilde{U}_{i+\frac{1}{2}}^\rho \right).$$

400 Following [30], the inequalities (3.7) hold under the linear sufficient condition

$$401 \quad \max\{0, A_{i+\frac{1}{2}}\} + |B_{i+\frac{1}{2}}| \leq C_{i+\frac{1}{2}},$$

402 if making use of $\theta_{i+\frac{1}{2}}^2 \leq \theta_{i+\frac{1}{2}}$, $\theta_{i+\frac{1}{2}} \in [0, 1]$. Thus the coefficient can be chosen as

$$403 \quad \theta_{i+\frac{1}{2}} = \min \left\{ 1, \frac{C_{i+\frac{1}{2}}}{\max\{0, A_{i+\frac{1}{2}}\} + |B_{i+\frac{1}{2}}|} \right\},$$

404 and the final limited numerical flux is

$$405 \quad (3.8) \quad \hat{F}_{i+\frac{1}{2}}^{\text{Lim}} = \hat{F}_{i+\frac{1}{2}}^{\text{L}} + \theta_{i+\frac{1}{2}} \Delta \hat{F}_{i+\frac{1}{2}}^{\text{Lim},*}.$$

406 **4. Scaling limiter for point value.** To achieve the BP property, it is also nec-
 407 essary to introduce BP limiting for the point value. As one will see in the numerical
 408 tests in Section 5, using power law reconstruction or BP limiting for cell average,
 409 individually or in combination, cannot guarantee the bounds. As there is no conser-
 410 vation requirement on the point value update, a simple scaling limiter [32] is directly
 411 performed on the high-order point values rather than on the flux for the cell average.

412 A first-order LLF scheme for the point value update can be

$$413 \quad (4.1) \quad U_{i+\frac{1}{2}}^{\text{L}} = U_{i+\frac{1}{2}}^n - \frac{2\Delta t^n}{\Delta x_i + \Delta x_{i+1}} \left(\hat{F}_{i+1}^{\text{L}}(U_{i+\frac{1}{2}}^n, U_{i+\frac{3}{2}}^n) - \hat{F}_i^{\text{L}}(U_{i-\frac{1}{2}}^n, U_{i+\frac{1}{2}}^n) \right),$$

414 with the numerical flux

$$415 \quad \hat{F}_i^{\text{L}}(U_{i-\frac{1}{2}}^n, U_{i+\frac{1}{2}}^n) = \frac{1}{2} \left(F(U_{i-\frac{1}{2}}^n) + F(U_{i+\frac{1}{2}}^n) \right) - \frac{\alpha_i}{2} \left(U_{i+\frac{1}{2}}^n - U_{i-\frac{1}{2}}^n \right),$$

$$416 \quad \alpha_i = \max\{\lambda(U_{i-\frac{1}{2}}^n), \lambda(U_{i+\frac{1}{2}}^n)\}.$$

418 Such an LLF scheme can be interpreted as a scheme on a staggered mesh if the point
 419 value is viewed as the cell average on the staggered mesh. Based on the proof in [34],
 420 it is straightforward to obtain the following Lemma.

421 LEMMA 4.1. The LLF scheme for the point value (4.1) is BP under the CFL
422 condition

$$423 \quad (4.2) \quad \Delta t^n \leq \frac{\Delta x_i + \Delta x_{i+1}}{4\alpha_i}.$$

424 The limited state is obtained by blending the high-order AF scheme (2.3) with
425 the forward Euler scheme and the LLF scheme (4.1) as $\mathbf{U}_{i+\frac{1}{2}}^{\text{Lim}} = \theta_{i+\frac{1}{2}} \mathbf{U}_{i+\frac{1}{2}}^{\text{H}} + (1 -$
426 $\theta_{i+\frac{1}{2}}) \mathbf{U}_{i+\frac{1}{2}}^{\text{L}}$, such that $\mathbf{U}_{i+\frac{1}{2}}^{\text{Lim}} \in \mathcal{G}$.

427 *Remark 4.2.* In the FVS for the point value update, the cell-centered value \mathbf{U}_i
428 is used. It is possible that $\mathbf{U}_i \notin \mathcal{G}$, then it is set as $\overline{\mathbf{U}}_i$ in such cases, which is a
429 reasonable second-order approximation.

430 **4.1. Application to scalar conservation laws.** This section enforces the
431 global MP $m_0 \leq u_{i+\frac{1}{2}}^{\text{Lim}} \leq M_0$ by choosing the coefficient as

$$432 \quad \theta_{i+\frac{1}{2}} = \begin{cases} \frac{u_{i+\frac{1}{2}}^{\text{L}} - m_0}{u_{i+\frac{1}{2}}^{\text{L}} - u_{i+\frac{1}{2}}^{\text{H}}}, & \text{if } u_{i+\frac{1}{2}}^{\text{H}} < m_0, \\ \frac{M_0 - u_{i+\frac{1}{2}}^{\text{L}}}{u_{i+\frac{1}{2}}^{\text{H}} - u_{i+\frac{1}{2}}^{\text{L}}}, & \text{if } u_{i+\frac{1}{2}}^{\text{H}} > M_0. \end{cases}$$

433 The final limited state is

$$434 \quad (4.3) \quad u_{i+\frac{1}{2}}^{\text{Lim}} = \theta_{i+\frac{1}{2}} u_{i+\frac{1}{2}}^{\text{H}} + (1 - \theta_{i+\frac{1}{2}}) u_{i+\frac{1}{2}}^{\text{L}}.$$

435 **4.2. Application to the compressible Euler equations.** The limiting con-
436 sists of two steps. First, the high-order state $\mathbf{U}_{i+\frac{1}{2}}^{\text{H}}$ is modified as $\mathbf{U}_{i+\frac{1}{2}}^{\text{Lim},*}$, such that its
437 density component satisfies $\mathbf{U}_{i+\frac{1}{2}}^{\text{Lim},*\rho} > \varepsilon$. Solving this inequality gives the coefficient

$$438 \quad \theta_{i+\frac{1}{2}}^* = \begin{cases} \frac{\mathbf{U}_{i+\frac{1}{2}}^{\text{L},\rho} - \varepsilon}{\mathbf{U}_{i+\frac{1}{2}}^{\text{L},\rho} - \mathbf{U}_{i+\frac{1}{2}}^{\text{H},\rho}}, & \text{if } \mathbf{U}_{i+\frac{1}{2}}^{\text{H},\rho} < \varepsilon, \\ 1, & \text{otherwise.} \end{cases}$$

439 Then the density component of the limited state is $\mathbf{U}_{i+\frac{1}{2}}^{\text{Lim},*\rho} = \theta_{i+\frac{1}{2}}^* \mathbf{U}_{i+\frac{1}{2}}^{\text{H},\rho} + (1 -$
440 $\theta_{i+\frac{1}{2}}^*) \mathbf{U}_{i+\frac{1}{2}}^{\text{L},\rho}$, with the other components remaining the same as $\mathbf{U}_{i+\frac{1}{2}}^{\text{H}}$.

441 Then the limited state $\mathbf{U}_{i+\frac{1}{2}}^{\text{Lim},*}$ is modified as $\mathbf{U}_{i+\frac{1}{2}}^{\text{Lim}}$, such that it gives positive
442 pressure, i.e., $p(\mathbf{U}_{i+\frac{1}{2}}^{\text{Lim}}) > \varepsilon$. Let $\mathbf{U}_{i+\frac{1}{2}}^{\text{Lim}} = \theta_{i+\frac{1}{2}}^{**} \mathbf{U}_{i+\frac{1}{2}}^{\text{Lim},*} + (1 - \theta_{i+\frac{1}{2}}^{**}) \mathbf{U}_{i+\frac{1}{2}}^{\text{L}}$. Note that the
443 pressure is a concave function (see e.g. [46]) of the conservative variables, such that

$$444 \quad p(\mathbf{U}_{i+\frac{1}{2}}^{\text{Lim}}) \geq \theta_{i+\frac{1}{2}}^{**} p(\mathbf{U}_{i+\frac{1}{2}}^{\text{Lim},*}) + (1 - \theta_{i+\frac{1}{2}}^{**}) p(\mathbf{U}_{i+\frac{1}{2}}^{\text{L}})$$

445 based on Jensen's inequality and $\mathbf{U}_{i+\frac{1}{2}}^{\text{Lim},*\rho} > 0$, $\mathbf{U}_{i+\frac{1}{2}}^{\text{L},\rho} > 0$, $\theta_{i+\frac{1}{2}}^{**} \in [0, 1]$. Thus a
446 sufficient condition is

$$447 \quad \theta_{i+\frac{1}{2}}^{**} = \begin{cases} \frac{p(\mathbf{U}_{i+\frac{1}{2}}^{\text{L}}) - \varepsilon}{p(\mathbf{U}_{i+\frac{1}{2}}^{\text{L}}) - p(\mathbf{U}_{i+\frac{1}{2}}^{\text{Lim},*})}, & \text{if } p(\mathbf{U}_{i+\frac{1}{2}}^{\text{Lim},*}) < \varepsilon, \\ 1, & \text{otherwise.} \end{cases}$$

448 The final limited state is

$$449 \quad (4.4) \quad \mathbf{U}_{i+\frac{1}{2}}^{\text{Lim}} = \theta_{i+\frac{1}{2}}^{**} \mathbf{U}_{i+\frac{1}{2}}^{\text{Lim},*} + \left(1 - \theta_{i+\frac{1}{2}}^{**}\right) \mathbf{U}_{i+\frac{1}{2}}^{\text{L}}.$$

450 Let us summarize the main results of the BP AF methods in this paper.

451 **THEOREM 4.3.** If the initial numerical solution $\overline{\mathbf{U}}_i^0, \mathbf{U}_{i+\frac{1}{2}}^0 \in \mathcal{G}$ for all i , and the
452 time step size satisfies (3.3) and (4.2), then the AF methods (2.2)-(2.3) equipped with
453 the SSP-RK3 (2.16) and the BP limitings

- 454 • (3.6) and (4.3) preserve the maximum principle for scalar case;
- 455 • (3.8) and (4.4) preserve the density and pressure positivity for the Euler equations.

456 **5. Numerical results.** This section conducts some numerical tests to verify
457 the accuracy of using the FVS for point value updates, the BP property, and the
458 shock-capturing ability of our AF methods.

459 **5.1. Scalar conservation laws.** This section shows the results for the linear
460 advection equation and the Burgers' equation, which demonstrate that the proposed
461 limiting can preserve the MP and suppress oscillations well.

462 *Example 5.1* (Advection equation). Consider the 1D advection equation $u_t + u_x =$
463 0 , on the periodic domain $[-1, 1]$ with the initial data [28]

$$464 \quad \begin{cases} \frac{1}{6} (G_1(x, \beta, z - \delta) + G_1(x, \beta, z + \delta) + 4G_1(x, \beta, z)), & \text{if } -0.8 \leq x \leq -0.6, \\ 1, & \text{if } -0.4 \leq x \leq -0.2, \\ 1 - |10(x - 0.1)|, & \text{if } 0 \leq x \leq 0.2, \\ \frac{1}{6} (G_2(x, \alpha, a - \delta) + G_2(x, \alpha, a + \delta) + 4G_2(x, \alpha, a)), & \text{if } 0.4 \leq x \leq 0.6, \\ 0, & \text{otherwise,} \end{cases}$$

465 where $G_1(x, \beta, z) = \exp(-\beta(x - z)^2)$, $G_2(x, \alpha, a) = \sqrt{\max(1 - \alpha^2(x - a)^2, 0)}$, and the
466 constants are $a = -0.5, z = -0.7, \delta = 0.005, \alpha = 10, \beta = \ln 2 / (36\delta^2)$. The problem is
467 solved for one period, i.e., until $T = 2$.

468 For the advection equation, the JS and LLF FVS are equivalent. The maximal
469 CFL number leading to a stable simulation is 0.41 without any limiting, and it reduces
470 to 0.13 when only the power law reconstruction is activated, and it increases a little
471 bit to 0.42 when only the BP limitings are used. When the power law reconstruction
472 and the BP limitings are employed together, the maximal CFL number can be 0.4.
473 The reduction of the CFL number with the power law reconstruction for semi-discrete
474 AF has, in fact, not been noticed previously. Thus, in the following simulations we
475 try not to use the power law reconstruction unless otherwise stated.

476 The results obtained with different limitings are shown in Figure 2, which are
477 computed with 400 cells and the CFL number is 0.1. The ranges of the numerical
478 solutions are listed in Table 1, considering both the cell averages and point values.
479 One can observe that there are some oscillations near the discontinuities without
480 any limiting, and that the power law reconstruction can eliminate the oscillations
481 effectively but is still not BP. The activation of either the BP limiting for the cell
482 average alone or the BP limiting for the point value alone also fails to preserve the
483 bounds $[0, 1]$, as one can see from Table 1, as is the case when using both the BP
484 limiting for the cell average and the power law reconstruction in the point value
485 update. Only when a BP limiting is performed on both the cell average and the
486 point value, the BP property is achieved, showing that using the two BP limitings

487 simultaneously is necessary for the preservation of the MP. **Figure 2** also shows the
 488 results obtained by imposing the global or local MP for the cell average, and global
 489 MP for the point value (without power law reconstruction), indicating that the use of
 490 local MP tends to dissipate the numerical solutions near the discontinuities and clip
 491 maxima more than the global MP.

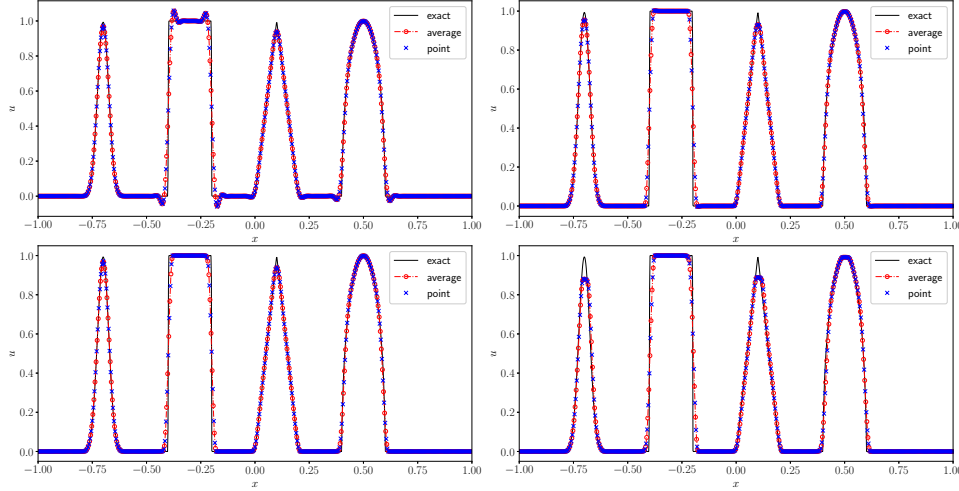


Fig. 2: **Example 5.1**, advection. The results are obtained without any limiting (upper left), with power law reconstruction (upper right), with BP limitings imposing global MP for the cell average and point value (lower left), with BP limitings imposing local and global MP for the cell average and point value (lower right).

none	$[-5.9 \times 10^{-2}, 1 + 5.9 \times 10^{-2}]$	✗
PLR	$[-2.7 \times 10^{-3}, 1 + 2.6 \times 10^{-3}]$	✗
global MP for average	$[-1.7 \times 10^{-3}, 1 + 1.7 \times 10^{-3}]$	✗
local MP for average	$[-1.3 \times 10^{-3}, 1 + 1.3 \times 10^{-3}]$	✗
global MP for point	$[-3.0 \times 10^{-4}, 1 + 2.6 \times 10^{-4}]$	✗
PLR + global MP for average	$[-9.8 \times 10^{-6}, 1 + 2.7 \times 10^{-6}]$	✗
PLR + local MP for average	$[-1.4 \times 10^{-5}, 1 + 1.9 \times 10^{-5}]$	✗
global MP for average + global MP for point	$[0.0, 1.0]$	✓
local MP for average + global MP for point	$[0.0, 1 - 9.4 \times 10^{-13}]$	✓
PLR + global MP for average + global MP for point	$[0.0, 1 - 1.1 \times 10^{-16}]$	✓
PLR + local MP for average + global MP for point	$[0.0, 1 - 7.3 \times 10^{-14}]$	✓

Table 1: **Example 5.1**, advection. The ranges of the numerical solutions (including both the cell averages and the point values) obtained with different limitings after one period. “PLR” denotes the power law reconstruction.

492 *Example 5.2* (Self-steepening shock). Consider the 1D Burgers’ equation $u_t +$
 493 $(\frac{1}{2}u^2)_x = 0$ on the domain $[-1, 1]$ with periodic boundary conditions. This test is
 494 solved until $T = 0.5$ with the initial condition as a square wave

$$u_0(x) = \begin{cases} 2, & \text{if } |x| < 0.2, \\ -1, & \text{otherwise.} \end{cases}$$

496 **Figures 3 and 4** plot the cell averages and point values based on different point
 497 value updates with 200 cells, as well as the reference solution. The spike generation
 498 has been observed in [26], and the reason is also discussed in **Subsection 2.2**. Such
 499 spike generation cannot be eliminated by using the power law reconstruction, nor do
 500 both BP limitings help to eliminate artefacts, as can be seen from **Figure 3**. The
 501 numerical solutions based on the LLF or SW FVS are shown in **Figure 4**, in which no
 502 spike appears. There are some oscillations near the discontinuity without limitings,
 503 and the numerical solutions agree well with the reference solution when the limitings
 504 are activated.

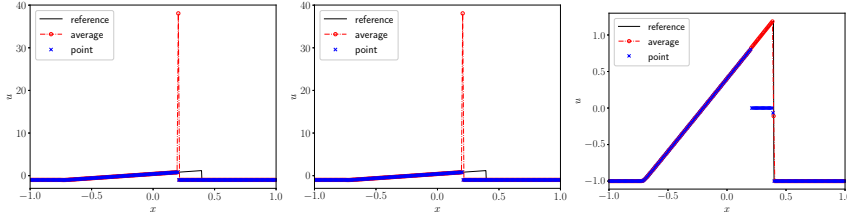


Fig. 3: Example 5.2, self-steepening shock for the Burgers' equation. The numerical solutions are based on the JS. From left to right: without limiting, with the power law reconstruction, with the BP limitings imposing local and global MP for the cell average and point value update, respectively.

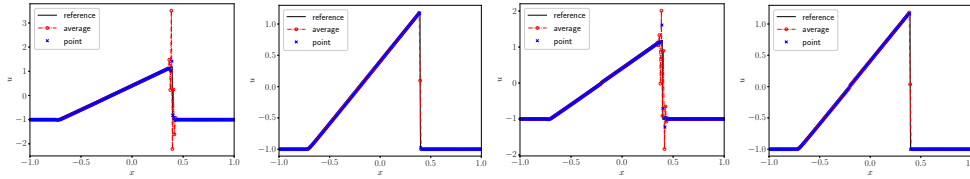


Fig. 4: Example 5.2, self-steepening shock for the Burgers' equation. From left to right: the LLF FVS without limiting, the LLF FVS with limitings, the SW FVS without limiting, the SW FVS with limitings. The limitings consider the local and global MP for the cell average and point value updates, respectively.

505 **5.2. The compressible Euler equations.** This section shows some challeng-
 506 ing tests, which require the BP property of the numerical methods in order to prevent
 507 simulations from crashing at some time. The adiabatic index is $\gamma = 1.4$ unless other-
 508 wise stated. Note that the BP limiting naturally reduces some oscillations.

509 *Example 5.3* (1D accuracy test for the Euler equations). This test is used to
 510 examine the accuracy of using different point value updates. The domain is $[0, 1]$ with
 511 periodic boundary conditions. Two manufactured solutions are constructed by adding
 512 additional source terms \mathbf{S} to the Euler equations,

$$\begin{aligned}
 (5.1) \quad \rho &= 4 + 0.1s_1, \quad v_1 = s_1, \quad p = (6002 + 398c_2 + 305s_1 + 5s_3)/1000, \\
 \mathbf{S} &= (\pi(39c_1 + s_2))/5, \quad -\pi(905c_1 + 15c_3 - 776s_2)/125, \\
 &\quad \pi c_1(20421 + 1179c_2 + 2160s_1 + 20s_3)/500,
 \end{aligned}$$

517 and

518 (5.2) $\rho = 4 + 0.1s_1, v_1 = 2 + 0.5s_1, p = (12328 + 472c_2 - 5455s_1 + 5s_3)/4000,$
 519 $S = (\pi(42c_1 + s_2)/10, \pi(4855c_1 - 15c_3 + 914s_2)/500,$
 520 $\pi c_1(14991 + 369c_2 - 2983s_1 + 5s_3)/1000),$

522 with $s_k = \sin(2k\pi(x - t)), c_k = \cos(2k\pi(x - t)), k = 1, 2, 3.$ The source terms are
 523 discretized by using Simpson’s rule for the cell average update. The problem is solved
 524 until $T = 0.4.$

525 In this test, the maximal CFL number is around 0.18 for the VH FVS, while
 526 around 0.43 for the JS, LLF, and SW FVS, thus we run the test with the same CFL
 527 number as 0.18. Figure 5 shows the following errors and corresponding convergence
 528 rates for the conservative variables in the ℓ^1 norm. It is seen that for the first exact
 529 solution (5.1), the JS and all the FVS except for the SW FVS achieve the designed
 530 third-order accuracy, while the SW FVS only gives second-order accuracy. Figure 6
 531 plots the density and velocity profiles obtained by the SW FVS with 80 cells. One
 532 can observe some defects in the density when the velocity is zero, similar to the “sonic
 533 point glitch” in the literature [38]. For the second exact solution (5.2), the velocity
 534 stays away from zero and no such issue appears. One possible reason is that the SW
 535 FVS is based on the absolute value of the eigenvalues, which is not smooth when the
 536 velocity is zero. Such an issue remains to be further explored in the future.

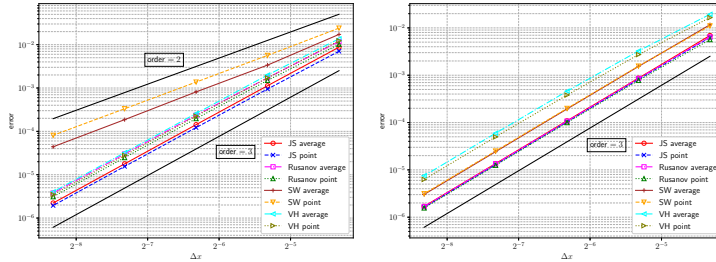


Fig. 5: Example 5.3, the accuracy tests for the 1D Euler equations based on the manufactured solutions (5.1) and (5.2) for the left and right plots, respectively.

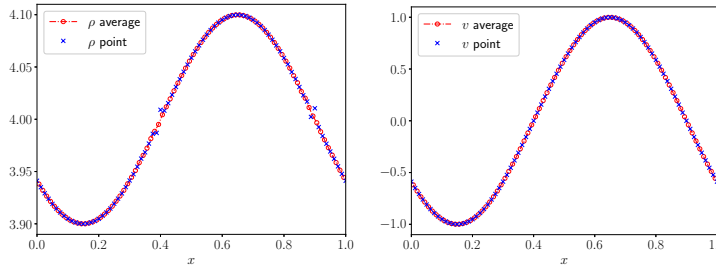


Fig. 6: Example 5.3, the density (left) and velocity (right) are obtained with the SW FVS and 80 cells for the 1D Euler equations based on the initial data (5.1).

537 *Example 5.4* (Double rarefaction problem). The exact solution to this problem
 538 contains a vacuum, so that it is often used to verify the BP property of numerical
 539 methods. The test is solved on a domain $[0, 1]$ until $T = 0.3$ with the initial data

$$540 \quad (\rho, v, p) = \begin{cases} (7, -1, 0.2), & \text{if } x < 0.5, \\ (7, 1, 0.2), & \text{otherwise.} \end{cases}$$

541 In this test, the AF method based on any kind of point value update mentioned
 542 in this paper gives negative density or pressure without the BP limitations. **Figure 7**
 543 shows the density computed with 400 cells and the BP limitations for the cell average
 544 and point value updates. The power law reconstruction is not used in this test, and
 545 the CFL number is 0.4 for all kinds of point value updates, except for 0.1 for the VH
 546 FVS. One observes that the BP AF method gets good performance for this example.

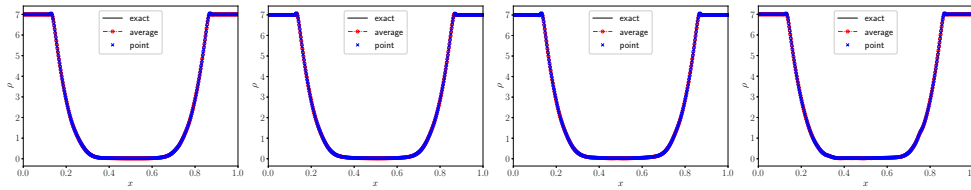


Fig. 7: **Example 5.4**, double rarefaction Riemann problem. The numerical solutions are computed with BP limitations for the cell average and point value updates on a uniform mesh of 400 cells. The power law reconstruction is not used. From left to right: JS, LLF, SW, and VH FVS.

547 *Example 5.5* (LeBlanc shock tube). This is a Riemann problem with an extremely
 548 large initial pressure ratio. This test is solved until $T = 5 \times 10^{-6}$ on a domain $[0, 1]$
 549 with the initial data

$$550 \quad (\rho, v, p) = \begin{cases} (2, 0, 10^9), & \text{if } x < 0.5, \\ (10^{-3}, 0, 1), & \text{otherwise.} \end{cases}$$

551 Without the BP limitations, the simulation will stop due to negative density or
 552 pressure. **Figure 8** shows the density computed on a uniform mesh of 400 and 6000 cells
 553 with the BP limitations for the cell average and point value updates. The CFL number
 554 is 0.4 for the LLF and SW FVS, and 0.15 for the JS and VH FVS for stability when
 555 the power law reconstruction is not used. It is seen that the numerical solutions on the
 556 coarse mesh deviate from the exact solutions, which has also been observed in other
 557 high-order BP methods, e.g., [45]. As the number of the mesh cells increases from 400
 558 to 6000, one can observe from **Figure 8** that the numerical solutions converge to the
 559 exact solutions with only a few overshoots/undershoots at the contact discontinuity.
 560 The LLF and SW FVS give better results.

561 To verify whether the power law reconstruction can suppress spurious oscillations
 562 and overshoots/undershoots, we rerun the test with the CFL number 0.1, and the
 563 density profiles are shown in **Figure 9**. It is obvious that only reducing the CFL
 564 number does not change the numerical solutions much except that the oscillations
 565 near the contact discontinuity based on the VH FVS are damped. When the power
 566 law reconstruction is activated, the overshoots/undershoots are reduced for the JS,

567 LLF, and SW FVS, while the VH FVS gives worse results even with a smaller CFL
 568 number (e.g. 0.02, not shown here), which needs further investigation.

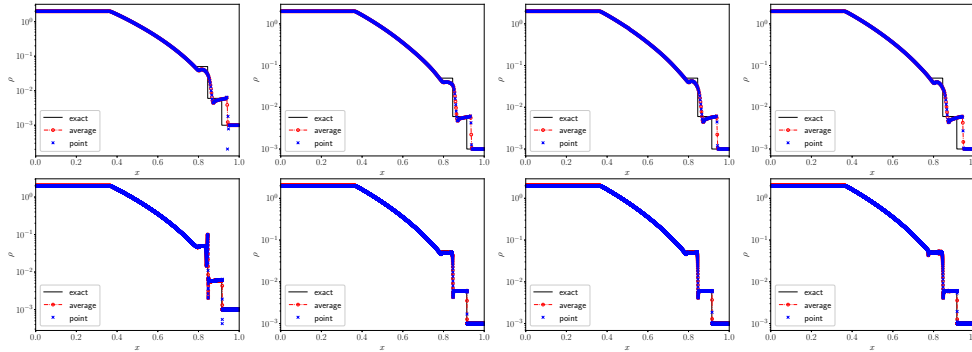


Fig. 8: **Example 5.5**, LeBlanc Riemann problem. The numerical solutions are computed with the BP limitings for the cell average and point value updates on a uniform mesh of 400 cells (top) and 6000 cells (bottom). The CFL number is 0.4 and the power law reconstruction is not used. From left to right: JS, LLF, SW, and VH FVS.

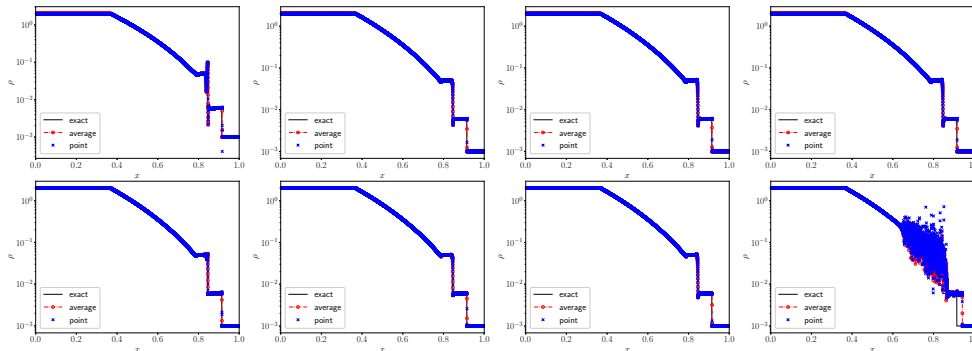


Fig. 9: **Example 5.5**, LeBlanc Riemann problem. The numerical solutions are computed with the BP limitings for the cell average and point value updates on a uniform mesh of 6000 cells. From left to right: JS, LLF, SW, and VH FVS. The CFL number is 0.1 and the power law reconstruction is not activated (top) and activated (bottom).

569 *Example 5.6* (Sedov problem). In this problem, a volume of uniform density and
 570 temperature is initialized, and a large quantity of thermal energy is injected at the
 571 center, developing into a blast wave that evolves in time in a self-similar fashion [36].
 572 An exact analytical solution based on self-similarity arguments is available [29], which
 573 contains very low density with strong shocks. The initial density is one, velocity is
 574 zero, and total energy is 10^{-12} everywhere except that in the center cell, the total
 575 energy of the cell average and point values at two cell interfaces are $3.2 \times 10^6 / \Delta x$
 576 with $\Delta x = 4/N$ with N the number of cells, which is used to emulate a δ -function at
 577 the center. The test is solved until $T = 5 \times 10^{-6}$.

578 This test is run with $N = 801$ cells, and the density plots in the right half domain
 579 are shown in **Figure 10**. The BP limitings are adopted for the cell average and point

580 value updates, while the power law reconstruction is not used. The maximal CFL
 581 numbers for different point value updates to be stable are also listed in the caption,
 582 i.e., 0.1 for the JS, 0.4, 0.3, and 0.25 for the LLF, SW, and VH FVS, respectively.
 583 The numerical solutions obtained by the three FVS are nearly the same, while there
 584 are some defects in the solution based on the JS. Thus the LLF FVS is superior to
 585 others regarding the time step size and the shock-capturing ability.

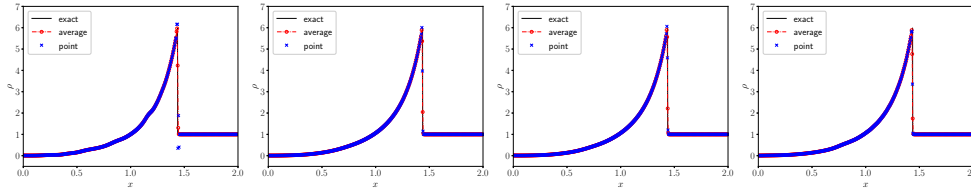


Fig. 10: [Example 5.6](#), Sedov problem. The numerical solutions are computed with the BP limitings for the cell average and point value updates on a uniform mesh of 801 cells, without the power law reconstruction. The CFL number is (from left to right): 0.1 for the JS, 0.4 for the LLF FVS, 0.3 for the SW FVS, 0.25 for the VH FVS.

586 *Example 5.7* (Blast wave interaction [\[42\]](#)). This test describes the interaction of
 587 two strong shocks in the domain $[0, 1]$ with reflective boundary conditions. The test
 588 is solved until $T = 0.038$.

589 Due to the low-pressure region, the schemes blow up without the BP limitings.
 590 [Figure 11](#) shows the density profiles and corresponding enlarged views in
 591 $x \in [0.62, 0.82]$ obtained by using the BP limitings on a uniform mesh of 800 cells,
 592 in which the power law reconstruction is not activated. It is seen that the numerical
 593 solutions are close to the reference solution, although there are some oscillations in
 594 the enlarged views. Then the power law reconstruction is additionally adopted to
 595 see if it can suppress the oscillations. The results with the CFL number 0.1 and a
 596 refined mesh of 1600 cells are shown in [Figure 12](#), from which one can observe that
 597 the oscillations reduce, and the LLF FVS gives the best result.

598 *Remark 5.8.* In the numerical tests, the maximal CFL numbers for stability are
 599 obtained by experiments. Note that the constraints [\(3.3\)](#) and [\(4.2\)](#) are used to guar-
 600 antee the BP property, while the reduction of the CFL numbers is due to the stability
 601 issue for different FVS and power law reconstruction.

602 **6. Conclusion.** In the active flux (AF) methods, the way how point values at
 603 cell interfaces are updated is essential to achieve stability and high-order accuracy.
 604 The point value update based on Jacobian splitting (JS) may lead to the so-called
 605 transonic issue for nonlinear problems due to inaccurate estimation of the upwind di-
 606 rection. This paper proposed to use the flux vector splitting (FVS) for the point value
 607 update instead of the JS, which keeps the continuous reconstruction as the original AF
 608 methods, and offers a natural and uniform remedy to the transonic issue. To further
 609 improve the robustness of the AF methods, this paper developed bound-preserving
 610 (BP) AF methods for general one-dimensional hyperbolic conservation laws, achieved
 611 by blending the high-order AF methods with the first-order local Lax-Friedrichs (LLF)
 612 or Rusanov methods for both the cell average and point value updates, where the con-
 613 vex limiting and scaling limiter were employed, respectively. For scalar conservation
 614 laws, the blending coefficient was determined based on the global or local maximum

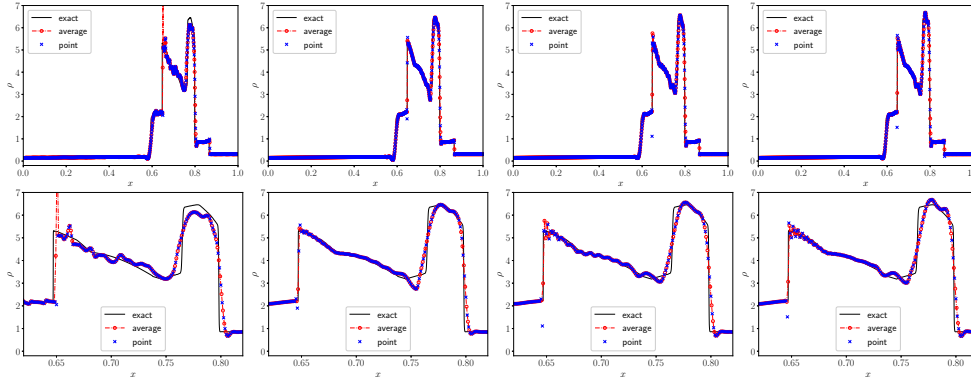


Fig. 11: [Example 5.7](#), blast wave interaction. The numerical solutions are computed with the BP limitings for the cell average and point value updates on a uniform mesh of 800 cells. The power law reconstruction is not used, and from left to right: the CFL number is 0.4, 0.4, 0.4, 0.35 for the JS, LLF, SW, and VH FVS, respectively. The corresponding enlarged views in $[0.62, 0.82]$ are shown in the bottom row.

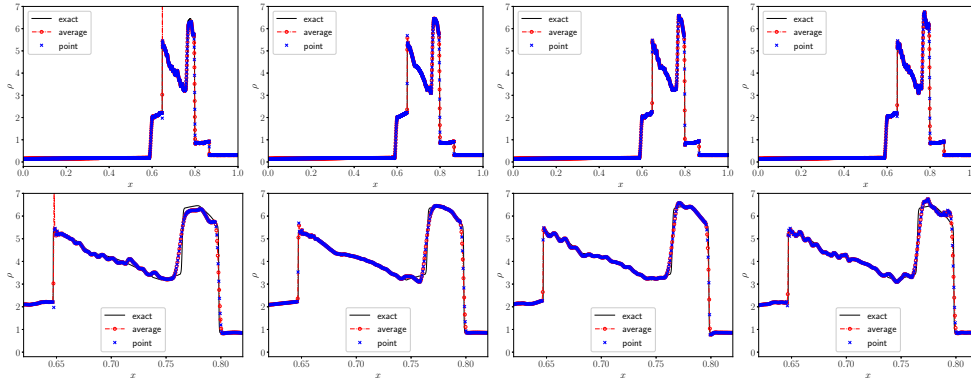


Fig. 12: [Example 5.7](#), blast wave interaction. The numerical solutions are computed with the power law reconstruction and the BP limitings for the cell average and point values update on a uniform mesh of 1600 cells. The CFL number is 0.1 for all the point value updates, and the corresponding enlarged views in $[0.62, 0.82]$ are shown in the bottom row. From left to right: JS, LLF, SW, and VH FVS.

615 principle, while for the compressible Euler equations, it was obtained by enforcing
 616 the positivity of density and pressure. Some challenging benchmark tests were con-
 617 ducted based on different choices of the point value update, including the JS, LLF,
 618 Steger-Warming, and Van Leer-Hänel FVS. The numerical results confirmed the ac-
 619 curacy, BP property, and shock-capturing ability of our methods, and also showed
 620 that the LLF FVS is generally superior to others in terms of the CFL number and
 621 shock-capturing ability. Our future work will include, among others, extending the
 622 current BP limitings to two-dimensional cases. We may also explore other ways to
 623 further suppress oscillations for the Euler equations.

- 625 [1] R. ABGRALL, *A combination of residual distribution and the active flux formulations or a*
626 *new class of schemes that can combine several writings of the same hyperbolic problem:*
627 *Application to the 1D Euler equations*, Commun. Appl. Math. Comput., 5 (2023), pp. 370–
628 402.
- 629 [2] R. ABGRALL AND W. BARSUKOW, *Extensions of active flux to arbitrary order of accuracy*,
630 ESAIM: Math. Model. Numer. Anal., 57 (2023), pp. 991–1027.
- 631 [3] R. ABGRALL, J. LIN, AND Y. LIU, *Active flux for triangular meshes for compressible flows*
632 *problems*, Dec. 2023, <https://arxiv.org/abs/2312.11271>.
- 633 [4] R. ABGRALL, W. BARSUKOW, AND C. KLINGENBERG, *The Active Flux method for the Euler*
634 *equations on Cartesian grids*, Oct. 2023, <https://arxiv.org/abs/2310.00683>.
- 635 [5] W. BARSUKOW, *The active flux scheme for nonlinear problems*, J. Sci. Comput., 86 (2021),
636 p. 3.
- 637 [6] W. BARSUKOW AND J. P. BERBERICH, *A well-balanced active flux method for the shallow*
638 *water equations with wetting and drying*, Commun. Appl. Math. Comput., (2023).
- 639 [7] W. BARSUKOW, J. P. BERBERICH, AND C. KLINGENBERG, *On the active flux scheme for*
640 *hyperbolic PDEs with source terms*, SIAM J. Sci. Comput., 43 (2021), pp. A4015–A4042.
- 641 [8] W. BARSUKOW, J. HOHM, C. KLINGENBERG, AND P. L. ROE, *The active flux scheme on*
642 *Cartesian grids and its low Mach number limit*, J. Sci. Comput., 81 (2019), pp. 594–622.
- 643 [9] E. CHUDZIK, C. HELZEL, AND D. KERKMANN, *The Cartesian grid active flux method: Linear*
644 *stability and bound preserving limiting*, Appl. Math. Comput., 393 (2021), p. 125501.
- 645 [10] S. CLAIN, S. DIOT, AND R. LOUBÈRE, *A high-order finite volume method for systems of con-*
646 *servation laws—Multi-dimensional Optimal Order Detection (MOOD)*, J. Comput. Phys.,
647 230 (2011), pp. 4028–4050.
- 648 [11] C. J. COTTER AND D. KUZMIN, *Embedded discontinuous Galerkin transport schemes with*
649 *localised limiters*, J. Comput. Phys., 311 (2016), pp. 363–373.
- 650 [12] C. M. DAFERMOS, *Hyperbolic Conservation Laws in Continuum Physics*, Springer Berlin Hei-
651 delberg, 2000.
- 652 [13] T. EYMANN AND P. ROE, *Active flux schemes*, in 49th AIAA Aerospace Sciences Meeting
653 including the New Horizons Forum and Aerospace Exposition, Orlando, Florida, Jan. 2011,
654 American Institute of Aeronautics and Astronautics.
- 655 [14] T. EYMANN AND P. ROE, *Active flux schemes for systems*, in 20th AIAA Computational Fluid
656 Dynamics Conference, Fluid Dynamics and Co-located Conferences, American Institute of
657 Aeronautics and Astronautics, June 2011.
- 658 [15] T. A. EYMANN AND P. L. ROE, *Multidimensional active flux schemes*, in 21st AIAA Computa-
659 tional Fluid Dynamics Conference, Fluid Dynamics and Co-located Conferences, American
660 Institute of Aeronautics and Astronautics, June 2013.
- 661 [16] D. FAN AND P. L. ROE, *Investigations of a new scheme for wave propagation*, in 22nd AIAA
662 Computational Fluid Dynamics Conference, American Institute of Aeronautics and Astro-
663 nautics, 2015.
- 664 [17] S. GOTTLIEB, C.-W. SHU, AND E. TADMOR, *Strong Stability-Preserving High-Order Time*
665 *Discretization Methods*, SIAM Rev., 43 (2001), pp. 89–112.
- 666 [18] J.-L. GUERMOND, M. NAZAROV, B. POPOV, AND I. TOMAS, *Second-order invariant domain*
667 *preserving approximation of the Euler equations using convex limiting*, SIAM J. Sci. Com-
668 put., 40 (2018), pp. A3211–A3239.
- 669 [19] J.-L. GUERMOND AND B. POPOV, *Fast estimation from above of the maximum wave speed in*
670 *the Riemann problem for the Euler equations*, J. Comput. Phys., 321 (2016), pp. 908–926.
- 671 [20] J.-L. GUERMOND AND B. POPOV, *Invariant domains and first-order continuous finite element*
672 *approximation for hyperbolic systems*, SIAM J. Numer. Anal., 54 (2016), pp. 2466–2489.
- 673 [21] J.-L. GUERMOND AND B. POPOV, *Invariant domains and second-order continuous finite ele-*
674 *ment approximation for scalar conservation equations*, SIAM J. Numer. Anal., 55 (2017),
675 pp. 3120–3146.
- 676 [22] J.-L. GUERMOND, B. POPOV, AND I. TOMAS, *Invariant domain preserving discretization-*
677 *independent schemes and convex limiting for hyperbolic systems*, Comput. Methods Appl.
678 Mech. Engrg., 347 (2019), pp. 143–175.
- 679 [23] H. HAJDUK, *Monolithic convex limiting in discontinuous Galerkin discretizations of hyperbolic*
680 *conservation laws*, Comput. Math. Appl., 87 (2021), pp. 120–138.
- 681 [24] D. HÄNEL, R. SCHWANE, AND G. SEIDER, *On the accuracy of upwind schemes for the solution*
682 *of the Navier-Stokes equations*, Fluid Dynamics and Co-located Conferences, American
683 Institute of Aeronautics and Astronautics, June 1987.
- 684 [25] A. HARTEN, P. D. LAX, AND B. V. LEER, *On upstream differencing and Godunov-type*

- 685 *schemes for hyperbolic conservation laws*, SIAM Rev., 25 (1983), pp. 35–61.
- 686 [26] C. HELZEL, D. KERKMANN, AND L. SCANDURRA, *A new ADER method inspired by the active*
687 *flux method*, J. Sci. Comput., 80 (2019), pp. 1463–1497.
- 688 [27] X. Y. HU, N. A. ADAMS, AND C.-W. SHU, *Positivity-preserving method for high-order con-*
689 *servative schemes solving compressible Euler equations*, J. Comput. Phys., 242 (2013),
690 pp. 169–180.
- 691 [28] G. S. JIANG AND C. W. SHU, *Efficient implementation of weighted ENO schemes*, J. Comput.
692 Phys., 126 (1996), pp. 202–228.
- 693 [29] J. R. KAMM AND F. X. TIMMES, *On efficient generation of numerically robust Sedov solutions*,
694 Tech. Report LA-UR-07-2849, 2007.
- 695 [30] D. KUZMIN, *Monolithic convex limiting for continuous finite element discretizations of hyper-*
696 *bolic conservation laws*, Comput. Methods Appl. Mech. Engrg., 361 (2020), p. 112804.
- 697 [31] D. KUZMIN, R. LÖHNER, AND S. TUREK, eds., *Flux-Corrected Transport: Principles, Algo-*
698 *rithms, and Applications*, Scientific Computation, Springer Netherlands, Dordrecht, 2012.
- 699 [32] X.-D. LIU AND S. OSHER, *Nonoscillatory high order accurate self-similar maximum principle*
700 *satisfying shock capturing schemes I*, SIAM J. Numer. Anal., 33 (1996), pp. 760–779.
- 701 [33] C. LOHMANN, D. KUZMIN, J. N. SHADID, AND S. MABUZA, *Flux-corrected transport algo-*
702 *rithms for continuous Galerkin methods based on high order Bernstein finite elements*, J.
703 Comput. Phys., 344 (2017), pp. 151–186.
- 704 [34] B. PERTHAME AND C.-W. SHU, *On positivity preserving finite volume schemes for Euler equa-*
705 *tions*, Numer. Math., 73 (1996), pp. 119–130.
- 706 [35] P. ROE, *Is discontinuous reconstruction really a good idea?*, J. Sci. Comput., 73 (2017),
707 pp. 1094–1114.
- 708 [36] L. I. SEDOV, *Similarity and Dimensional Methods in Mechanics*, Academic Press, New York,
709 1959.
- 710 [37] J. L. STEGER AND R. F. WARMING, *Flux vector splitting of the inviscid gasdynamic equations*
711 *with application to finite-difference methods*, J. Comput. Phys., 40 (1981), pp. 263–293.
- 712 [38] H. TANG, *On the sonic point glitch*, J. Comput. Phys., 202 (2005), pp. 507–532.
- 713 [39] E. F. TORO, *Riemann Solvers and Numerical Methods for Fluid Dynamics*, Springer Berlin
714 Heidelberg, 2009.
- 715 [40] B. VAN LEER, *Towards the ultimate conservative difference scheme. IV. A new approach to*
716 *numerical convection*, J. Comput. Phys., 23 (1977), pp. 276–299.
- 717 [41] B. VAN LEER, *Flux-vector splitting for the Euler equations*, in Eighth International Conference
718 on Numerical Methods in Fluid Dynamics, E. Krause, ed., Lecture Notes in Physics, Berlin,
719 Heidelberg, 1982, Springer, pp. 507–512.
- 720 [42] P. WOODWARD AND P. COLELLA, *The numerical simulation of two-dimensional fluid flow*
721 *with strong shocks*, J. Comput. Phys., 54 (1984), pp. 115–173.
- 722 [43] K. WU AND C.-W. SHU, *Geometric quasilinearization framework for analysis and design of*
723 *bound-preserving schemes*, SIAM Rev., 65 (2023), pp. 1031–1073.
- 724 [44] Z. XU, *Parametrized maximum principle preserving flux limiters for high order schemes solving*
725 *hyperbolic conservation laws: one-dimensional scalar problem*, Math. Comput., 83 (2014),
726 pp. 2213–2238.
- 727 [45] X. ZHANG AND C.-W. SHU, *On positivity-preserving high order discontinuous Galerkin*
728 *schemes for compressible Euler equations on rectangular meshes*, J. Comput. Phys., 229
729 (2010), pp. 8918–8934.
- 730 [46] X. ZHANG AND C.-W. SHU, *Maximum-principle-satisfying and positivity-preserving high-order*
731 *schemes for conservation laws: survey and new developments*, Proceedings of the Royal
732 Society A: Mathematical, Physical and Engineering Sciences, 467 (2011), pp. 2752–2776.
- 733 [47] X. ZHANG AND C.-W. SHU, *Positivity-preserving high order discontinuous Galerkin schemes*
734 *for compressible Euler equations with source terms*, J. Comput. Phys., 230 (2011),
735 pp. 1238–1248.